

Algorithms and Code for the Generation of Generalized Monkhorst-Pack Grids

Yunzhe Wang¹, Pandu Wisesa¹, Adarsh Balasubramanian¹, Shyam Dwaraknath² and Tim Mueller^{1,*}

¹ Department of Materials Science and Engineering, Johns Hopkins University, Baltimore, Maryland 21218, USA

² Lawrence Berkeley National Laboratory, Berkeley, California, 94720, USA

E-mail: tmueller@jhu.edu

Abstract

Computational modeling of the properties of crystalline materials has become an increasingly important research paradigm over the last decade. A routine operation in such calculations is the evaluation of integrals over the Brillouin zone, where traditional Monkhorst-Pack grids are widely used across popular simulation packages. We have previously demonstrated that generalised Monkhorst-Pack k -point grids, which are generated independently of any particular choice of reciprocal lattice unit cell, are much more efficient than traditional Monkhorst-Pack grids and can roughly double the speed of well-converged calculations of the properties of crystalline materials. In this paper, we present algorithms that can rapidly generate optimized generalized Monkhorst Pack grids both dynamically and using a pre-generated database. The algorithms identify highly efficient grids by performing an exhaustive search over all symmetry-preserving grids, and they also incorporate designs to accelerate such searches. Implementations of these algorithms in three different formats are provided to meet the diverse demands of users. We present benchmarks of the speed of our algorithms on structures randomly selected from the Inorganic Crystal Structure Database. For grids that correspond to a real-space supercell with at least 50 angstroms between lattice points, which is sufficient to converge density functional theory calculations within 1 meV / atom for nearly all materials, our algorithm finds optimized grids in an average of 0.19 seconds on a single processing core. For 100 angstroms between real-space lattice points, our algorithm finds optimal grids in less than 5 seconds on average. Our benchmarks further show that the database

approach is consistently faster than dynamic grid generation, and the grids returned by our algorithms are more efficient than those generated by previously reported algorithms.

Keywords: Brillouin zone, k -points

1. Introduction

Computational materials research has become increasingly vital in probing the properties of crystalline materials, especially in screening materials at a large scale to accelerate material discoveries for a wide range of applications. A routine operation for calculating the properties of crystalline materials is the evaluation of integrations over the first Brillouin zone, which can be approximated by discretely sampling the Brillouin Zone at a set of points known as k -points. For most methods, the computational cost of a calculation scales linearly with the number of the symmetrically irreducible k -points used to approximate the integral.

Many popular computational materials software packages generate k -points using the Monkhorst-Pack scheme [1], which creates k -point grids that are regular and aligned with the reciprocal lattice vectors. In an $m_1 \times m_2 \times m_3$ Monkhorst-Pack grid, the coordinates of the k -points are given by

$$\mathbf{k} = \frac{n_1}{m_1} \mathbf{b}_1 + \frac{n_2}{m_2} \mathbf{b}_2 + \frac{n_3}{m_3} \mathbf{b}_3 + \mathbf{s}, \quad n_1 = 0 \dots m_1 - 1, \quad n_2 = 0 \dots m_2 - 1, \quad n_3 = 0 \dots m_3 - 1 \quad (1)$$

where m_1 , m_2 , and m_3 are positive integers, \mathbf{b}_1 , \mathbf{b}_2 and \mathbf{b}_3 are reciprocal lattice vectors, and \mathbf{s} represents a shift vector that moves the grid away from the origin (known as the Γ point in reciprocal space). There exists a mapping between each regular k -point grid and a real-space superlattice that defines the Born-von Karman boundary conditions for the periodicity of the wave functions [2, 3]. The superlattice corresponding to the k -point grid defined by equation (1) is given by

$$(\mathbf{g}_1, \mathbf{g}_2, \mathbf{g}_3)^T = \mathbf{M}(\mathbf{a}_1, \mathbf{a}_2, \mathbf{a}_3)^T \quad (2)$$

where \mathbf{a}_1 , \mathbf{a}_2 , and \mathbf{a}_3 represent the real-space primitive lattice vectors, \mathbf{g}_1 , \mathbf{g}_2 , and \mathbf{g}_3 represent the lattice vectors of the superlattice, and the transformation matrix \mathbf{M} is equal to

$$\mathbf{M} = \begin{bmatrix} m_1 & 0 & 0 \\ 0 & m_2 & 0 \\ 0 & 0 & m_3 \end{bmatrix}. \quad (3)$$

The reciprocal primitive lattice vectors share an analogous relationship with those of the reciprocal superlattice. The reciprocal lattice vectors of a direct lattice are calculated by

$$[\mathbf{b}_1, \mathbf{b}_2, \mathbf{b}_3]^T = [\mathbf{a}_1, \mathbf{a}_2, \mathbf{a}_3]^{-1} \quad (4)$$

where the vectors share the same definition as in equations (1) and (2). Similarly, the primitive reciprocal lattice vectors of the superlattice can be obtained by

$$[\mathbf{d}_1, \mathbf{d}_2, \mathbf{d}_3]^T = [\mathbf{g}_1, \mathbf{g}_2, \mathbf{g}_3]^{-1} \quad (5)$$

where \mathbf{d}_1 , \mathbf{d}_2 , and \mathbf{d}_3 are the reciprocal lattice vectors corresponding to the direct superlattice. Substituting equations (4) and (5) into equation (2), the following relationship can be derived:

$$[\mathbf{b}_1, \mathbf{b}_2, \mathbf{b}_3]^T = \mathbf{M}^T [\mathbf{d}_1, \mathbf{d}_2, \mathbf{d}_3]^T. \quad (6)$$

The matrix multiplication order implies that the row vectors of the matrix \mathbf{M}^T contain the coordinates of the vectors $\{\mathbf{b}_1, \mathbf{b}_2, \mathbf{b}_3\}$ in the basis of $\{\mathbf{d}_1, \mathbf{d}_2, \mathbf{d}_3\}$.

In terms of the matrix \mathbf{M} , equation (1) can be written as

$$\begin{aligned} \mathbf{k} &= (n_1, n_2, n_3) \left(\begin{bmatrix} m_1 & 0 & 0 \\ 0 & m_2 & 0 \\ 0 & 0 & m_3 \end{bmatrix}^{-1} \right)^T (\mathbf{b}_1, \mathbf{b}_2, \mathbf{b}_3)^T + \mathbf{s} \\ &= (n_1, n_2, n_3) (\mathbf{M}^{-1})^T (\mathbf{b}_1, \mathbf{b}_2, \mathbf{b}_3)^T + \mathbf{s} \\ &= (n_1, n_2, n_3) [\mathbf{d}_1, \mathbf{d}_2, \mathbf{d}_3]^T + \mathbf{s} \end{aligned} \quad (7)$$

Therefore, the set of vectors $\{\mathbf{d}_1, \mathbf{d}_2, \mathbf{d}_3\}$ are a generating basis of the k -point grid. As shown in equation (7), the traditional Monkhorst-Pack scheme uses a diagonal matrix \mathbf{M} , which is equivalent to the constraint that the k -point grids are aligned with the reciprocal lattice vectors. However Froyen has pointed out that this constraint is not necessary [4], and we have previously demonstrated that much more efficient grids can be generated if the Monkhorst-Pack approach is generalized by relaxing this requirement [5].

The isomorphism between a k -point grid and a superlattice in direct space suggests that the minimum spacing between points on a superlattice, $r_{lattice}$, is a good descriptor of the accuracy of a density functional theory (DFT) calculation using the corresponding k -point grid [4]. A rigorous justification for the adoption of this descriptor for semiconductors and insulators has been laid out in our previous work [5], where we showed that the integration error due to approximating the integral by a discrete sum over k -points is expected to decay exponentially with a decay rate approximately proportional to $r_{lattice}$. This insight is supported by a recent empirical study by Choudhary and Tavazza which indicates that this length-based descriptor for k -point density has smoother convergence in DFT calculations and stronger correlations with physical parameters of materials over a measurement based on the total number of k -points per reciprocal atom [6]. Based on this insight, we developed a publicly accessible server that returns to the user the optimal generalized k -point grid that minimizes the number of irreducible k -points (computational cost) for a given value of $r_{lattice}$ (desired accuracy) [5]. The server is backed by a database of pre-calculated grids for all systems other than triclinic and monoclinic, for which generalized k -point grids are generated dynamically. The use of this approach has been shown to reduce the computational cost for well-converged calculations by a factor of approximately 2 compared to regular Monkhorst-Pack grids [5, 7].

In the years since our previous work was published there has been increasing interest in the generation and use of generalized k -point grids [6, 8-26]. Of particular note, Hart and co-workers have recently developed algorithms and released an open-source software package (GRkgridgen) for generating generalized k -point grids on the fly [27, 28]. Some of the core elements of these algorithms, such as the use of Hermite Normal Form to identify unique superlattices [29, 30], are similar to some of ours. However, there are some notable differences. In particular, we have developed algorithms that perform an exhaustive search for the symmetry-preserving grid that minimizes the number of irreducible k -points (computational cost) for a user-provided lower bound for $r_{lattice}$, which has been shown both theoretically [5] and empirically [6] to be a good descriptor of grid accuracy.

To facilitate the use of generalized k -point grids we have developed and present here algorithms for both on-the-fly grid generation and a database lookup that are optimized to quickly generate highly efficient generalized k -point grids. These algorithms are implemented in our sever as well as in two open-source tools we are releasing to the community. For the first tool, we have packaged our server into an open-source stand-alone application that is available at <https://gitlab.com/muellergroup/k-pointGridGenerator>. This application is self-contained and written in Java, and it can be run without the need for compilation or external library installation on any machine on which Java is installed. Like the server, the stand-alone

application dynamically generates grids for monoclinic and triclinic crystal systems and uses a database of pre-calculated grids for all others. This application can be downloaded and run locally without the need for an internet connection at run time. It contains all of the features of the server. We have also developed kpLib, a lightweight library written in C++ that dynamically generates grids on the fly, requiring only that the users provide information about the space group of the reciprocal lattice. This library is designed for integration with third-party applications and to be compatible with external software packages such as Spglib [31]. To maximize the efficiency of the tools, the algorithms applied are optimized based on a user-provided lower bound for $r_{lattice}$, which we refer to as r_{min} .

To illustrate the performance of the implementations, benchmarks are performed on various grid generation methods presented in this paper. The dynamic grid generation algorithm can identify the optimal grid for r_{min} up to 75 angstroms in less than 1 second on average, and the database approach is shown to be consistently faster than dynamic grid generation. It is also shown that the cost of using the generated grids, as determined by the number of irreducible k -points, is lower than that of grids with comparable density and r_{min} values generated using the GRkgridgen software package.

In the following sections, a detailed explanation of the core algorithms underlying these tools is provided. Next, the three implementations are briefly discussed. Lastly, various benchmarks of the speed of the algorithms and quality of the resulting grids are provided. A few other algorithms, which improve performance and add functionalities to our tools but are not essential in creating generalized k -point grids, are provided in the supplementary information.

2. Methodology

In this section we discuss the core algorithms behind our tools. We start by describing our approach for dynamically generating generalized grids, as this approach is used to populate the database, is adopted for monoclinic and triclinic crystal systems in all implementations, and is used for all grid generation by kpLib. We describe the algorithms for enumerating symmetry-preserving superlattices and for determining the symmetrically irreducible k -points and corresponding weights. Next, we provide an overview of the database lookup method. Lastly, we briefly describe how scale factors are used to accelerate the generation of large size grids.

In the following discussion, we use the symbols N_i and N_T to represent, respectively, the number of symmetrically irreducible k -points and the number of total k -points in the Brillouin zone. N_T is also then the number of primitive cells in a unit cell of the corresponding real-space superlattice (aka the “size” of the superlattice), and is given by the absolute value of the determinant of \mathbf{M} (equation (6)).

2.1 An Overview of the Dynamic Grid Generation Algorithm

The grid generation algorithm starts with three parameters describing the input structure:

1. The real-space primitive lattice vectors, $\{\mathbf{a}_1, \mathbf{a}_2, \mathbf{a}_3\}$.
2. The real-space conventional lattice vectors, where at least one of the vectors is orthogonal to the other two for all but triclinic systems. We label these $\{\mathbf{c}_1, \mathbf{c}_2, \mathbf{c}_3\}$.
3. The group of point symmetry operations, $\{\mathbf{R}\}$, that the k -point grid (and real-space superlattice) should preserve. These point symmetry operations can be generated by removing translation from all the operations in the real-space crystallographic space group. If the system has time reversal symmetry, then the reciprocal-space band structure will have inversion symmetry even if the real-space crystal does not. In this case, inversion and any additional operators required to complete the group should be added if they are not already present.

The algorithm searches for the k -point grid that minimizes N_i while satisfying the following two constraints:

1. $r_{lattice}$ for the corresponding superlattice not smaller than r_{min} (a value provided by the user),
2. N_T is greater than or equal to N_{min} (another value provided by the user).

Symmetry-preserving lattices, in which every symmetry operation maps a lattice point to another lattice point, usually result in the smallest values of N_i by maximizing the use of symmetry. Thus, the algorithm only searches over lattices that are symmetry-preserving.

We start by determining a lower bound for N_T , which we call, N_{lower} . It is the larger value of N_{min} and the minimum size that any superlattice can have with while satisfying $r_{lattice} \geq r_{min}$:

$$N_{lower} = \max\left(N_{min}, \left\lfloor \frac{\sqrt{2}}{2} r_{min}^3 / V_p \right\rfloor \right) \quad (8)$$

where V_p is the volume of the primitive cell, $\frac{\sqrt{2}}{2} r_{min}^3$ is the volume of a unit cell in a face-centered cubic (fcc) lattice for which the distance between lattice points is r_{min} , $\lfloor x \rfloor$ is the floor operation that returns the largest integer no greater than the argument x , and $\max()$ is a function that returns the argument with the maximum value. Equation (8) can be justified by considering that fcc structures maximize the packing density for rigid spheres [32] and thus $\frac{\sqrt{2}}{2} r_{min}^3$ is the minimum unit cell volume for a superlattice for which $r_{lattice}$ is at least r_{min} .

The search for optimal superlattices starts with lattices of size N_{lower} and generates symmetry-preserving superlattices using an algorithm to be introduced in section 2.3. For each symmetry-preserving superlattice, the scheme checks whether $r_{lattice}$ is smaller than r_{min} and discards it if it is. When the first superlattice for which $r_{lattice} \geq r_{min}$ is found, its corresponding k -point grid is kept as the initial “best grid”, and the scheme can determine an upper limit for the search, N_{upper} :

$$N_{upper} = N_i \times N_{sym} \quad (9)$$

where N_{sym} is the number of unique point symmetry operations for the system, as provided in the third input parameter listed above. Any superlattices with $N_T \geq N_{upper}$ would necessarily have more irreducible k -points than that of the initial best grid. If at some point a superlattice with N_i smaller than that of the best known grid is found, the best grid is updated to this newly found one and the value of N_{upper} is adjusted accordingly. When two k -point grids have the same N_i , the scheme favours the one with a larger $r_{lattice}$ in the corresponding superlattice. If $r_{lattice}$ of both superlattices also tie, the scheme chooses the one with a larger N_T . The search ends when the upper limit of the sizes of superlattices is reached. Figure 1 summarizes the steps of the scheme.

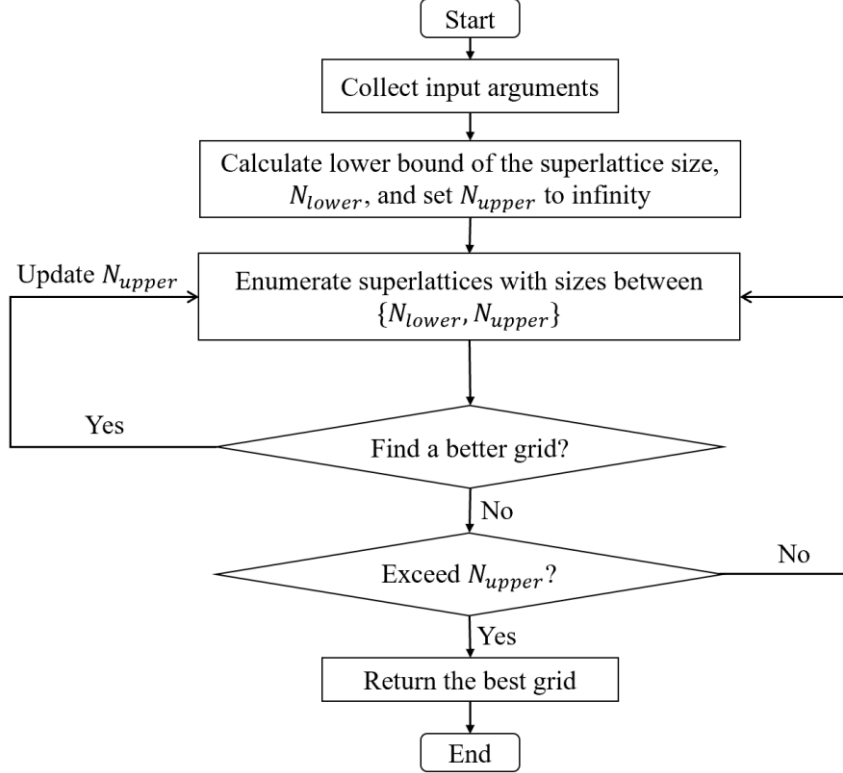


Figure 1. A diagram summarizes the workflow of the dynamic grid generation algorithm.

2.2 Representation of Superlattices and Identification of Symmetry-Preserving Superlattices

Each superlattice is represented by the Hermite normal form (HNF) [29, 30] of the transformation matrix, \mathbf{M} , where \mathbf{M} is as shown in equation (3). The Hermite normal form (\mathbf{H}) is defined for integral matrices and satisfies the following requirements

$$H_{ij} = 0, \text{ if } j > i \quad (10)$$

$$0 \leq H_{ij} < H_{jj}, \text{ if } j < i \quad (11)$$

Equation (10) states that a matrix in HNF is lower-triangular, and equation (11) requires that all elements are non-negative and the maximum element in each column resides on the diagonal. There is an equivalent upper-triangular formulation of the HNF of a matrix, but we use the lower-triangular one. Each non-singular integral matrix can be transformed into its Hermite normal form by multiplying a series of unimodular matrices (integral matrices whose determinant is 1 or -1). In other words, the determinant of a matrix and its HNF are equal. And it has been shown that two superlattices are equivalent if and only if

the HNF of their generation matrix \mathbf{M} are the same [29, 30]. An alternative, yet equivalent statement is that the HNF of a matrix is unique. The uniqueness of HNF of a matrix provides a convenient algorithm to enumerate all possible superlattices of a primitive lattice. The details have been laid out in references [29, 30]. We use a simple algorithm, developed from the uniqueness of the HNF of a matrix, to determine whether a superlattice preserves a given point symmetry operation. The algorithm works as follows:

- 1) Multiply the matrix representation of the point symmetry, \mathbf{R} , with the HNF, \mathbf{H} , of the transformation matrix, \mathbf{M} .
- 2) Find the HNF form of the resulting integral matrix from last step, \mathbf{H}' .
- 3) If $\mathbf{H} = \mathbf{H}'$, then this superlattice preserves this point operation \mathbf{R} . Otherwise, the superlattice doesn't possess this symmetry.

2.3 Algorithm for Efficient Enumeration of Symmetry-Preserving Superlattices

The efficiency of the returned generalize k -point grids relies on the exhaustiveness of the enumeration of all possible superlattices. Such computationally expensive enumeration has been identified as the main hurdle of applying generalized k -point grids in calculations of properties of crystalline materials [5, 33]. A rough estimation can show how the number of possible superlattices grows with lattice size. Given a size, N_T , of a superlattice, and a factorization of it into three distinct positive integers $\{N_1, N_2, N_3\}$, the number of unique matrices in HNF with the three numbers as the diagonal elements, would be

$$N_1^2 N_2 + N_2^2 N_1 + N_1^2 N_3 + N_3^2 N_1 + N_2^2 N_3 + N_3^2 N_2, \quad (12)$$

counting all permutations of the three numbers at the diagonal positions. The total number of possible superlattices can be calculated by considering all ways in which N_T can be factored into three numbers. For example, the total number of unique superlattices with a size of 1000, which is a typical number of the total number of k -points in calculations of metallic systems, is 3,147,430.

Morgan et al. have presented an algorithm for accelerating the enumeration of symmetry-preserving lattices for a given lattice size by expressing the primitive lattice in Niggli-reduced form [28]. For each of the 44 distinct Niggli bases, they have determined symmetry-based constraints on the entries of \mathbf{H} that can be used to reduce the number of possible lattices that must be considered. We have developed an

approach that similarly iterates over symmetry-preserving lattices, with two key differences: it does not rely on Niggli reduction, and it is optimized for grid selection based on r_{min} , which has been shown to work well as a descriptor of k -point density both in theory [5] and in practice [5, 6].

2.3.1 Crystal Systems Other than Triclinic

We start by considering systems that are not triclinic. For such systems at least one of the conventional lattice vectors must, by the symmetry of the system, be perpendicular to the other two. For simplicity, our only requirement is that such a vector be listed third, as \mathbf{c}_3 .

The key to our approach is the recognition that any regular three-dimensional lattice consists of layers of identical two-dimensional lattices that are normal to \mathbf{c}_3 . Each two-dimensional lattice may be shifted from the one below it by a constant shift vector that is parallel to its lattice plane, and for symmetry-preserving lattices only a finite set of shift vectors are allowed. For example, if there is a twofold rotational axis parallel to \mathbf{c}_3 , then this axis may only pass through points in the two-dimensional lattice formed by linear combinations of half lattice vectors (Table 1). Any other shift would result in a lattice that is not symmetry preserving. Similarly, if there is a mirror plane perpendicular to \mathbf{c}_3 , then either the mirror plane must be at the mid-point between two layers, in which case no shift is allowed, or it must pass through one of the layers, and again only the shifts shown in Table 1 are allowed. This concept is illustrated in two dimensions in Figure 2. Similar sets of shifts may be derived for three-fold rotational axes (Table 1).

A high-level summary of our algorithm for enumerating symmetry-preserving lattices is then as follows:

- 1) Determine all pairs of factors of the total lattice size. In each pair, the first factor represents the size of the supercell in each two-dimensional layer and the second represents the number of layers in each three-dimensional supercell.
- 2) For each pair of factors, enumerate all symmetry-preserving two-dimensional lattices with the required size.
- 3) Combine each two-dimensional lattice with each allowed shift to create a candidate three-dimensional lattice.
- 4) Verify that the three-dimensional lattice is symmetry-preserving as described above.

Table 1. Possible displacements of lattice planes in real space in 2 dimensions, and of the Γ point in reciprocal space in 3 dimensions.

Crystal System	Shift vectors in the basis of $\{\mathbf{c}_1, \mathbf{c}_2\}$ in real space	Shift vectors of the Γ point in the basis of $\{\mathbf{d}_1, \mathbf{d}_2, \mathbf{d}_3\}$ as defined in equation (5)
Cubic, Tetragonal, Orthorhombic, Monoclinic	$[0.0, 0.0], [0.0, 0.5], [0.5, 0.0], [0.5, 0.5]$	$[0.0, 0.0, 0.0], [0.0, 0.0, 0.5], [0.0, 0.5, 0.0], [0.5, 0.0, 0.0], [0.5, 0.5, 0.0], [0.5, 0.0, 0.5]$
Hexagonal, Trigonal	$[0.0, 0.0], [1/3, 0.0], [0.0, 1/3], [0.0, 2/3], [2/3, 0.0], [1/3, 1/3], [2/3, 2/3], [1/3, 2/3], [2/3, 1/3]$	$[0.0, 0.5, 0.5], [0.5, 0.5, 0.5]$

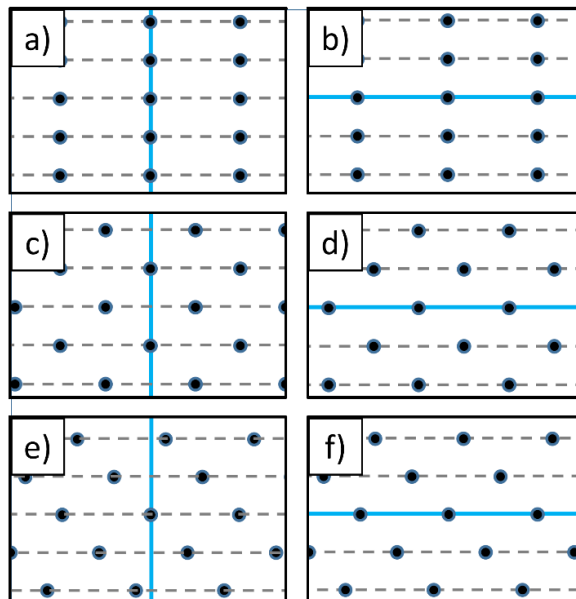


Figure 2. Two-dimensional examples of allowed and disallowed shifts. In all examples the blue line represents a mirror plane, black dots represent lattice points on the real-space superlattice, and the dashed lines show the different layers of lattice points that are orthogonal to \mathbf{c}_2 (which here serves the role that \mathbf{c}_3 serves in three dimensions). a), b), c), and d) show allowed shifts in which the mirror plane transforms every lattice point to another lattice point. In a) and b) there is zero shift, and in c) and d) the shift is half the real-space superlattice vector normal to \mathbf{c}_2 . e) and f) show disallowed shifts, as the mirror planes do not transform every lattice point to another lattice point.

This algorithm effectively reduces the problem of enumerating three-dimensional lattices to one of enumerating two-dimensional lattices, which significantly accelerates the search for symmetry-preserving lattices. We can further accelerate the search by recognizing that if the number of layers is too small to satisfy the requirement that $r_{lattice} \geq r_{min}$, we can skip the enumeration of two-dimensional lattices and move on to the next set of factors. Similarly, if we ever determine that the $r_{lattice} < r_{min}$ for any two-dimensional layer, then we can stop evaluation of all lattices constructed from that layer and move onto the next two-dimensional lattice. We find that pre-screening the lattices for $r_{lattice}$ in this way significantly increases the speed of the algorithm when r_{min} is the limiting factor, as demonstrated in benchmarking calculations in section 4.1.

Algorithm 1 Fast Enumeration of Symmetry-Preserving Superlattices

Input:

N_T - Size of superlattice. Also the total number of k -points in the grid.
 $\{\mathbf{c}_1, \mathbf{c}_2, \mathbf{c}_3\}$ - Conventional lattice vectors.
 $\{\mathbf{R}\}$ - The point symmetry group to be preserved in superlattices.
 $\{\mathbf{a}_1, \mathbf{a}_2, \mathbf{a}_3\}$ - Primitive lattice vectors.
 $\{\mathbf{s}\}$ - Array of possible 2D shift vectors.
 r_{min} - Minimum periodic distance specified by users.

Output:

$\{\{\mathbf{g}_1, \mathbf{g}_2, \mathbf{g}_3\}\}$ - Array of symmetry-preserving superlattices with $r_{lattice} \geq r_{min}$.

Initialization:

$\{\{\mathbf{g}_1, \mathbf{g}_2, \mathbf{g}_3\}\}$ - Empty array of symmetry-preserving superlattices.
 \mathbf{H} - A 2×2 zero matrix.
 \mathbf{M} - A 3×3 zero matrix.

```

1: find the point symmetry group,  $\{\mathbf{R}^{2D}\}$ , of the 2D sublattice  $\{\mathbf{c}_1, \mathbf{c}_2\}$ ;  

2: factorSets[][]  $\leftarrow$  sets of factorizations of  $N_T$  into 2 integral numbers;  

3: for factors[] in factorSets[][] do  

4:   primLayerSpacing =  $\|\mathbf{c}_3\| \times V_p/V_c$ ;  

5:   maxLayers = isHexagonal() ?  $3 : 2$ ;  

6:   maxZDistance = factors[2]  $\times$  primLayerSpacing  $\times$  maxLayers;  

7:   if maxZDistance  $< r_{min}$  then  

8:     continue;  

9:    $\{\{\mathbf{g}_1, \mathbf{g}_2\}\} \leftarrow$  initialize an empty array of 2 vectors;  

10:  factorSets2D[][]  $\leftarrow$  sets of factorization of factors[1] into 2 integral numbers;  

11:  for factors2D[] in factorSets2D[][] do  

12:     $H_{11} = \text{factors2D}[1], H_{22} = \text{factors2D}[2]$   

13:    for  $i = 0$  to factors2D[1] - 1 do  

14:       $H_{21} = i$ ;  

15:      if not symmetryPreserving( $\mathbf{H}, \{\mathbf{R}^{2D}\}$ ) then  

16:        continue;  

17:       $\mathbf{g}_1 = H_{11}\mathbf{c}_1$ ;  

18:       $\mathbf{g}_2 = H_{21}\mathbf{c}_1 + H_{22}\mathbf{c}_2$ ;  

19:      add  $\{\mathbf{g}_1, \mathbf{g}_2\}$  to the array of 2D symmetry-preserving superlattices,  $\{\{\mathbf{g}_1, \mathbf{g}_2\}\}$ ;  

20:    for  $\{\mathbf{g}_1, \mathbf{g}_2\}$  in  $\{\{\mathbf{g}_1, \mathbf{g}_2\}\}$  do  

21:      if getMinDistance( $\mathbf{g}_1, \mathbf{g}_2$ )  $< r_{min}$  then  

22:        continue;  

23:      for  $\mathbf{s}$  in  $\{\mathbf{s}\}$  do  

24:         $\mathbf{g}_3 = [s_1, s_2] \cdot [\mathbf{g}_1, \mathbf{g}_2]^T + (\text{factors}[2] / (V_c/V_p)) \cdot \mathbf{c}_3$ ;  

25:        if getMinDistance( $\mathbf{g}_1, \mathbf{g}_2, \mathbf{g}_3$ )  $< r_{min}$  then  

26:          continue;  

27:         $\mathbf{M} = [\mathbf{g}_1, \mathbf{g}_2, \mathbf{g}_3]^T \cdot ([\mathbf{a}_1, \mathbf{a}_2, \mathbf{a}_3]^T)^{-1}$ ;  

28:        if  $\mathbf{M}$  contains non-integral elements then  

29:          continue;  

30:        if not symmetryPreserving( $\mathbf{M}, \{\mathbf{R}\}$ ) then  

31:          continue;  

32:        add  $\{\mathbf{g}_1, \mathbf{g}_2, \mathbf{g}_3\}$  to the array of symmetry-preserving superlattices;  

33: return  $\{\{\mathbf{g}_1, \mathbf{g}_2, \mathbf{g}_3\}\}$ ;
  
```

Figure 3. Algorithm for fast enumeration of symmetry preserving superlattices for systems other than triclinic.

The steps of the algorithm are shown by the pseudocode in Figure 3. Some elaborations of the pseudocode are given below:

- The input conventional vectors should have \mathbf{c}_3 orthogonal to the other two vectors. In addition, if the two-dimensional unit cell defined by \mathbf{c}_1 and \mathbf{c}_2 has a point on the primitive lattice at its center, we replace \mathbf{c}_1 and \mathbf{c}_2 with a pair of primitive lattice vectors along the same plane. Thus $\{\mathbf{c}_1, \mathbf{c}_2\}$ always defines a primitive lattice in its residing lattice plane to ensure the algorithm can exhaustively search all possible superlattices by multiplying integral matrices.
- Line 2: Permutations of the same set of 2 factors are treated as different factorizations, i.e. $\{2, 3\}$ and $\{3, 2\}$ are two different factorizations of 6.
- The for loops in line 3, line 11, line 20 and line 23 means for each of the elements in the set, execute the loop once. At the end of each execution of the loop, the looping element is incremented. The “continue” in line 8, 16, 22, 26, 29 and 31 means skipping the remaining operations in the current loop and continuing the loop with the next element in the set.
- Line 4 – line 6: this block calculates the maximum possible length of the shortest vector parallel with \mathbf{c}_3 in a superlattice. V_c and V_p are volumes of the conventional and primitive unit cells, respectively. “primLayerSpacing” is the distance between adjacent layers of two-dimensional lattices. “maxLayers” is the maximum number of layers after which the stacking sequence starts to repeat. This value is 3 for lattices in hexagonal crystal system (including hexagonal and trigonal lattices) and 2 for other lattices. The reason for the differences is that lattices have different sets of two-dimensional shifts, as listed in Table 1.
- “isHexagonal() ? 3 : 2” represents a conditional operator and is an abbreviation of the statement “if isHexagonal() == true then 3 else 2”.
- Line 6: arrays in the pseudocode have their indices starting from 1. Therefore, “factor[2]” indicates the second factor of this factorization.
- Line 15 and line 30: the algorithm discussed in section 2.2 is used to determine whether a superlattice preserves the given group of point symmetries.
- Line 21 and line 25: “ $getMinDistance(\{\mathbf{g}_i\})$ ” is a function that uses Minkowski reduction [34] to determine the minimum distance between two lattice points in the lattice defined by $\{\mathbf{g}_i\}$. The input lattice can have any dimensionality up to three.

- Line 28: if \mathbf{M} has non-integral elements, then $\{\mathbf{g}_1, \mathbf{g}_2, \mathbf{g}_3\}$ is not a superlattice of the primitive lattice.

In addition to pre-screening for $r_{lattice}$, this algorithm accelerates the enumeration in several ways. Firstly, it drastically decreases the total number of 3-dimensional superlattices that need to be checked for symmetry preservation. Secondly, the groups of symmetry in 2-dimensional sublattice have fewer number of symmetry operations comparing with their corresponding groups in 3 dimensions. And thirdly, a 2-dimensional matrix multiplication takes fewer elementary operations than a 3-dimensional one.

Algorithm 2 Fast Enumeration of Symmetry-Preserving Superlattices for Triclinic Structures

Input:

N_T - Size of the superlattice. Also the total number of k -points in the grid.

r_{min} - Minimum periodic distance specified by users.

$\{\mathbf{a}_1, \mathbf{a}_2, \mathbf{a}_3\}$ - Primitive lattice vectors.

Output:

$\{\{\mathbf{g}_1, \mathbf{g}_2, \mathbf{g}_3\}\}$ - Array of symmetry-preserving superlattices with $r_{lattice} \geq r_{min}$.

Initialization:

\mathbf{H} - A 3×3 zero matrix.

$\{\{\mathbf{g}_1, \mathbf{g}_2, \mathbf{g}_3\}\}$ - Empty array of symmetry-preserving superlattices.

```

1: factorSets[][]  $\leftarrow$  sets of integral factorizations of  $N_T$  into 3 numbers;
2: for  $\{N_1, N_2, N_3\}$  in factorSets[][] do
3:    $\mathbf{H} \leftarrow$  put  $N_1, N_2, N_3$  on diagonal positions;
4:    $\mathbf{g}_1 = H_{11} \cdot \mathbf{a}_1$ ;
5:   if  $\|\mathbf{g}_1\| < r_{min}$  then
6:     continue;
7:   for  $H_{21} = 0$  to  $N_1 - 1$  do
8:      $\mathbf{g}_2 = H_{21} \cdot \mathbf{a}_1 + H_{22} \cdot \mathbf{a}_2$ ;
9:     if  $getMinDistance(\mathbf{g}_1, \mathbf{g}_2) < r_{min}$  then
10:      continue;
11:      for  $(H_{31}, H_{32}) = (0, 0)$  to  $(N_1 - 1, N_2 - 1)$  do
12:         $\mathbf{g}_3 = H_{31} \cdot \mathbf{a}_1 + H_{32} \cdot \mathbf{a}_2 + H_{33} \cdot \mathbf{a}_3$ ;
13:        if  $getMinDistance(\mathbf{g}_1, \mathbf{g}_2, \mathbf{g}_3) < r_{min}$  then
14:          continue;
15:        add  $\{\mathbf{g}_1, \mathbf{g}_2, \mathbf{g}_3\}$  to the array of superlattices;
16: return the array of superlattices;

```

Figure 4. Algorithm for enumerating symmetry-preserving superlattices for triclinic system, accelerated by enforcing $r_{lattice} \geq r_{min}$ at each dimension.

2.3.2 Triclinic Crystal System

The triclinic system doesn't benefit from the above algorithm since all its superlattices preserve the point symmetry operations of the primitive lattice, namely the identity operation and sometimes the inversion

operation. For triclinic systems we accelerate the search for superlattices for which $r_{lattice} \geq r_{min}$ by again considering one dimension at a time. For each factor set, if $H_{11}|\mathbf{a}_1| < r_{min}$, the shortest distance between lattice points must be less than r_{min} and the factor set is not considered. Similarly, if the two dimensional lattice spanned by $H_{11}\mathbf{a}_1$ and $H_{21}\mathbf{a}_1 + H_{22}\mathbf{a}_2$ has $r_{lattice} < r_{min}$ we do not iterate over possible values of H_{31} and H_{32} as we already know the lattices will not satisfy the required constraint. The procedures are summarized as a pseudo code in Figure 4. The input lattice can be of any dimension up to three. We note that a similar approach can be used to accelerate any scheme based on iterating over lattices in HNF, such as the one developed by Morgan et al. [28].

2.4 Evaluating Shift Vectors

K -point grids can be generated for each symmetry-preserving lattice using equation (7), where the matrix \mathbf{H} can be used for \mathbf{M} . The only remaining unknown in equation (7) is the shift vector \mathbf{s} . For a shift to be guaranteed to result in a symmetry-preserving lattice, it must shift the origin to a point that has the full point group symmetry of the origin. For all symmorphic space groups, the only such points are located at linear combinations of full- or half-multiples of the primitive lattice vectors. Thus, we consider only the eight such unique combination of k -point grid generating vectors, $\{\mathbf{d}_1, \mathbf{d}_2, \mathbf{d}_3\}$, as candidate shift vectors (Table 1). In some cases (e.g. hexagonal systems), some of the shift vectors in Table 1 will not result in a symmetry-preserving grid. We identify and reject these when determining the number of irreducible k -points. As this occurs as soon as the first point that breaks symmetry is encountered, it comes with relatively little computational cost.

2.5 Algorithms for Fast Calculation of Symmetrically Irreducible K -points and K -point Weights

We select the optimal lattice based on the values of N_i , $r_{lattice}$, and N_T . The value of $r_{lattice}$ can be easily obtained from the superlattice vectors by Minkowski reduction, and N_T equals the absolute value of the determinant of the transformation matrix \mathbf{M} . However, calculating N_i for a k -point grid is a relatively expensive operation. An intuitive approach is to apply all the point symmetry operations to each k -point, \mathbf{k}_i , and compare the resulting coordinates with all the other k -points. If one of the transformed k -points,

\mathbf{k}_i' , is translationally equivalent to one of the other k -points, \mathbf{k}_j , then the k -points \mathbf{k}_i and \mathbf{k}_j are symmetrically equivalent. However, this algorithm scales as $O(N_T^2)$, where N_T is the number of total k -points of a grid. As this operation is applied to each of the k -point grids found by the algorithm in section 2.3, this intuitive but costly approach could easily become the major overhead of any k -point generation scheme.

We solve this complication by first recognizing that a unit cell in reciprocal space is a supercell of a regular k -point lattice, where the two lattices are related by equation (6). The matrix \mathbf{M}^T is the transpose of the matrix used to construct the real-space superlattice that corresponds to the k -point grid. We transform \mathbf{M}^T to Hermite normal form. To avoid confusion with the Hermite normal form of \mathbf{M} , which we have labelled \mathbf{H} , we will refer to the Hermite normal form of \mathbf{M}^T as \mathbf{J} . We note that in general, \mathbf{J} does not have to be equal to \mathbf{H}^T . The key to our approach is the recognition that it is possible to tessellate all of reciprocal space with supercells of size $J_{11} \times J_{22} \times J_{33}$ arranged periodically on the superlattice, where J_{11} , J_{22} , and J_{33} are the diagonal elements of \mathbf{J} and each lattice point is a corner of the supercell. This is illustrated in two dimensions in Figure 5, but the same concept extends to any number of dimensions. The off-diagonal elements of \mathbf{J} serve to shift each layer of supercells relative to the previous layer, so that the tessellation resembles stacked bricks. Within each of these supercells, the coordinates of a k -point can be expressed as:

$$\mathbf{r} + ([k_1, k_2, k_3] + \mathbf{s}) \cdot [\mathbf{d}_1, \mathbf{d}_2, \mathbf{d}_3]^T \quad (13)$$

where \mathbf{r} is a lattice point on the reciprocal space lattice (blue dots in Figure 5), \mathbf{d}_1 , \mathbf{d}_2 , and \mathbf{d}_3 are generating lattice vectors of the k -point lattice (also reciprocal primitive lattice vectors), k_1 is an integer from 0 to $J_{11} - 1$, k_2 is an integer from 0 to $J_{22} - 1$, and k_3 is an integer from 0 to $J_{33} - 1$. The coordinates of the k -point can then be easily transformed into any basis (such as that of the primitive lattice in reciprocal space) using linear operations. We have shared this approach for iterating over k -points with the Hart group for their work with generalized k -point grids [27]. Values for k_1 , k_2 , and k_3 can be quickly calculated for any k -point using integer arithmetic, as shown by lines 15 and 16 in Figure 6 and discussed below.

Given the enumeration of k -points using equation (13), we identify irreducible k -points in a way similar to that described by Hart et al. [27]. We assign a unique index to each k -point in the Brillouin zone or,

equivalently, to each k -point in any unit cell of the reciprocal lattice. The values of the index range from 1 to N_T , and translationally equivalent k -points share the same index. Linear scaling is achieved because the index for any given k -point can be calculated in constant time, as can the sublattice of k -points that have a given index. Indices are assigned to k -points using

$$\text{index} = 1 + k_1 + J_{11}k_2 + J_{11}J_{22}k_3. \quad (14)$$

Then iteration of all k -points in a unit cell in reciprocal space, equivalent to all k -points in the Brillouin zone, is accomplished by looping over values of k_1 , k_2 , and k_3 in equation (14).

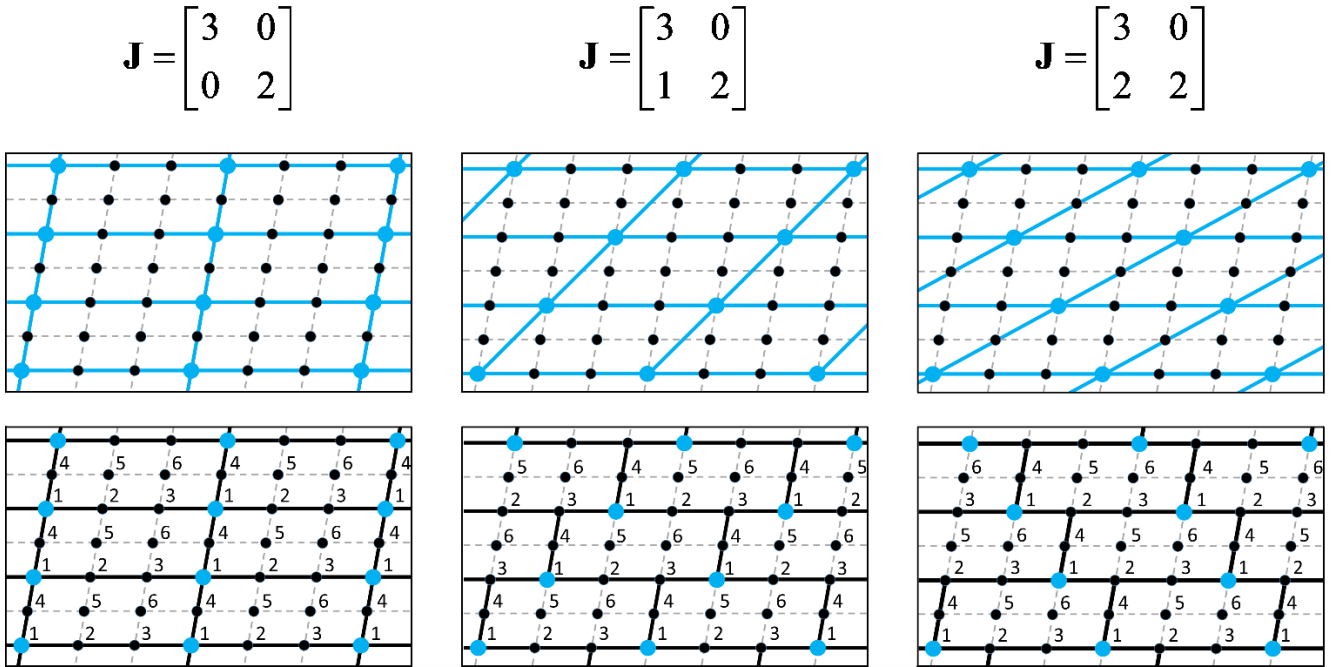


Figure 5. Two-dimensional illustrations of the concepts used for k -point enumeration and index generation. The top row provides the three possible matrices in Hermite normal form for the set of factors (3,2). The middle row shows the three Bravais superlattices corresponding to these matrices, assuming that the generating vectors for the k -point grid, \mathbf{d}_1 and \mathbf{d}_2 , are aligned with the dashed gray lines. The bottom row shows how space can be tessellated by unit cells that are 3×2 supercells of the generating lattice vectors, where each unit cell is associated with a point on the superlattice (in the lower-left corner of the cell). The k -point indices within each cell, as would be calculated by the two-dimensional equivalent of equation (14), are shown.

To count the number of distinct k -points, we iterate over all translationally distinct k -points as described above and apply all symmetry operations to each k -point. If an operation does not transform the k -point to another k -point, the grid is not symmetry-preserving and is rejected (this can sometimes happen if a shift

breaks symmetry). If the index of any symmetrically equivalent k -point is less than that of the current k -point, then we have already seen a symmetrically equivalent k -point, so the counter for the number of irreducible k -points is not incremented. If there is no symmetrically equivalent k -point with an index lower than that of the current k -point, then the current k -point is the first we've seen in its orbit, so the counter for the number of irreducible k -points is incremented. A simple variation of this algorithm is used to calculate k -point weights by, for each k -point, determining the orbit of symmetrically equivalent points and then incrementing the weight of the k -point that has the lowest index in that orbit. Figure 6 provides the pseudocode of this algorithm.

Algorithm 3 Fast calculation of symmetrically irreducible k -points and k -points weights

Input:

$\{\mathbf{R}\}$ - The point symmetry group of the symmorphic space group of input structure.
 \mathbf{H} - The transformation matrix of real-space superlattice in Hermite normal form.
 N_T - Number of total k -points for the grid to be calculated for.
 \mathbf{s} - Shift vector of the Γ point.

Output:

N_i - Number of symmetrically irreducible k -point.
coordinates[N_T][3] - Array of k -point coordinates.
weights[N_T] - Array of weights.

Initialization:

$\{\mathbf{R}'\}$ - Empty array of 3x3 matrices, representing symmetry operation in the basis of generating vectors, $\{\mathbf{d}_1, \mathbf{d}_2, \mathbf{d}_3\}$.
 $N_i = 0$.
coordinates[N_T][3] - Zero array of coordinates.
weights[N_T] - Zero array.

```
1: for  $\mathbf{R}$  in  $\{\mathbf{R}\}$  do
2:    $\mathbf{R}' = \mathbf{H}^T \cdot (\mathbf{R}^T)^{-1} \cdot (\mathbf{H}^T)^{-1}$ ;
3:   add  $\mathbf{R}'$  to the array,  $\{\mathbf{R}'\}$ ;
4:  $\mathbf{J} \leftarrow$  HNF of  $\mathbf{H}^T$ ;
5: let  $\mathbf{J} = [\mathbf{j}_1, \mathbf{j}_2, \mathbf{j}_3]^T$ ;
6: for  $k_3 = 0$  to  $J_{33} - 1$  do
7:   for  $k_2 = 0$  to  $J_{22} - 1$  do
8:     for  $k_1 = 0$  to  $J_{11} - 1$  do
9:       index =  $1 + k_1 + J_{11}k_2 + J_{11}J_{22}k_3$ ;
10:      minIndex  $\leftarrow$  initialize as infinity;
11:      for  $\mathbf{R}'$  in  $\{\mathbf{R}'\}$  do
12:         $[k'_1, k'_2, k'_3] = [[k_1, k_2, k_3] + \mathbf{s}] \cdot \mathbf{R}' - \mathbf{s}$ ;
13:        if  $[k'_1, k'_2, k'_3]$  contains non-integral values then
14:          return 0, null, null;
15:          for  $i = 3$  to 1 do
16:             $[k'_1, k'_2, k'_3] = [k'_1, k'_2, k'_3] - \lfloor k'_i/J_{ii} \rfloor \cdot \mathbf{j}_i$ ;
17:            newIndex =  $1 + k'_1 + J_{11}k'_2 + J_{11}J_{22}k'_3$ ;
18:            minIndex =  $\min(\minIndex, newIndex)$ ;
19:             $[x_1, x_2, x_3] = ([k_1, k_2, k_3] + \mathbf{s}) \cdot (\mathbf{H}^T)^{-1}$ ;
20:             $\mathbf{k} = [x_1 \% 1, x_2 \% 1, x_3 \% 1]$ ;
21:            coordinates[index] =  $\mathbf{k}$ ;
22:            if  $\minIndex == index$  then
23:               $N_i = N_i + 1$ ;
24:              weights[index] = 1;
25:            else
26:              weights[minIndex] = weights[minIndex] + 1;
27: return  $N_i$ , coordinates[ ][3], weights[ ];
```

Figure 6. Algorithm for fast calculation the coordinates of symmetrically irreducible k -points and the corresponding weights.

Some explanations are provided as follows:

- Line 12 – line 14: this code block determines whether a given shift vector preserves all the point symmetries. The idea is that the resulting k -point, from applying firstly a shift and then a symmetry

operation, should also be a k -point that is generated by shifting another k -point. Hence if the coordinates of the resulting point expressed in the basis of the k -point lattice, $[k_1', k_2', k_3']$, are not integers then the point is not a point on the grid. As soon as the first point that does not preserve symmetry is identified, the algorithm returns empty results and terminates the remaining steps.

- Line 15 – line 16: this is the reverse operation of equation (13) in the basis of the reciprocal primitive lattice. Given a k -point, it finds the integral coordinates of the translationally equivalent k -point within the unit cell located at the origin. $\lfloor k_i' / J_{ii} \rfloor$ represents the floor operation, which returns the greatest integer no larger than the argument.
- Line 19 – line 21: changes the basis of the k -point coordinates to the reciprocal superlattice vectors, $\{\mathbf{b}_1, \mathbf{b}_2, \mathbf{b}_3\}$, which is the reciprocal lattice of the input primitive lattice.
- Line 20: “%” represents the modulo operation. This operation shifts all the coordinates to their equivalent ones within the supercell defined by $\{\mathbf{b}_1, \mathbf{b}_2, \mathbf{b}_3\}$.
- Line 27: the returned arrays contain coordinates and weights for all k -point. The symmetrically non-distinct points, however, have weights of zero. This fact is used to identify the subset of irreducible points.

2.6 An Overview of the Database Search Algorithm

Section 2.1 to section 2.5 describe algorithms for dynamical generation of the optimal k -point grid. To further accelerate the search of the optimal grid, we have employed the above algorithms to generate a database of optimal grids. The use of this database can significantly speed up the generation of a generalized k -point grid. A brief description of the database has been presented in our previous work [5]. The database currently contains 428,632 pre-calculated symmetry-preserving grids, both shifted and Γ -centered, covering each of the 21 centrosymmetric space groups other than triclinic and monoclinic ones. The number of grids has increased by 637%, compared with the database used in our previous work [5] as we have increased grid density and the number of shift vectors considered. The maximum size of stored k -point grids has increased from 1,728 ($12 \times 12 \times 12$) to 5,832 ($18 \times 18 \times 18$) for orthorhombic, tetragonal, trigonal and hexagonal systems. The maximum size for cubic systems has grown to 46,656 ($36 \times 36 \times 36$). The grids for each of these space groups are stored in 42 separate binary files (21 for shifted and 21 for Γ -centered grids). Figure 7 gives a schematic outline of the database organization.

The database groups grids with the same N_i and the same symmetry group in one array, and indexes arrays by N_i to accelerate the search for grids with minimal N_i . Each grid in the database has fields for N_T , N_i , the generating matrix \mathbf{H} of its corresponding superlattice, the shift $\mathbf{H}r_{lattice}$ vector, and a set of coefficients for fast estimation of $r_{lattice}$. A unique index is used to represent \mathbf{H} , generated using the same mechanism as used for iterating over superlattices described in section 2.3. The matrix can be easily recovered from the index. Memory is saved by storing only an integer instead of an array of nine numbers.

The sets of coefficients assigned to each lattice represent linear combinations of a set of pre-defined lattice vectors that have been previously found to generate the shortest lattice vector for some set of lattice parameters. These coefficients are used to quickly determine an upper bound for $r_{lattice}$. If this upper bound is smaller than r_{min} , we skip the grid and move on to the next. Otherwise, Minkowski reduction is used to find explicitly the shortest real-space lattice vector, and if it has a length of less than r_{min} then the set of coefficients is updated. In this way the search algorithm learns from experience and becomes more efficient the more it is used.

When generating generalized k -point grids by searching the database, a procedure similar to that of the dynamic search is used. The difference is that the iteration of grids changes from explicitly constructing grids at each value of N_T to a simple, constant-time lookup of entries in each array indexed by N_i . Detailed descriptions of the algorithms for mapping each \mathbf{H} to a unique index and estimating $r_{lattice}$ from sets of coefficients, as well as a diagram showing the workflow of the database search approach, are given in section 2 of the supplementary information.

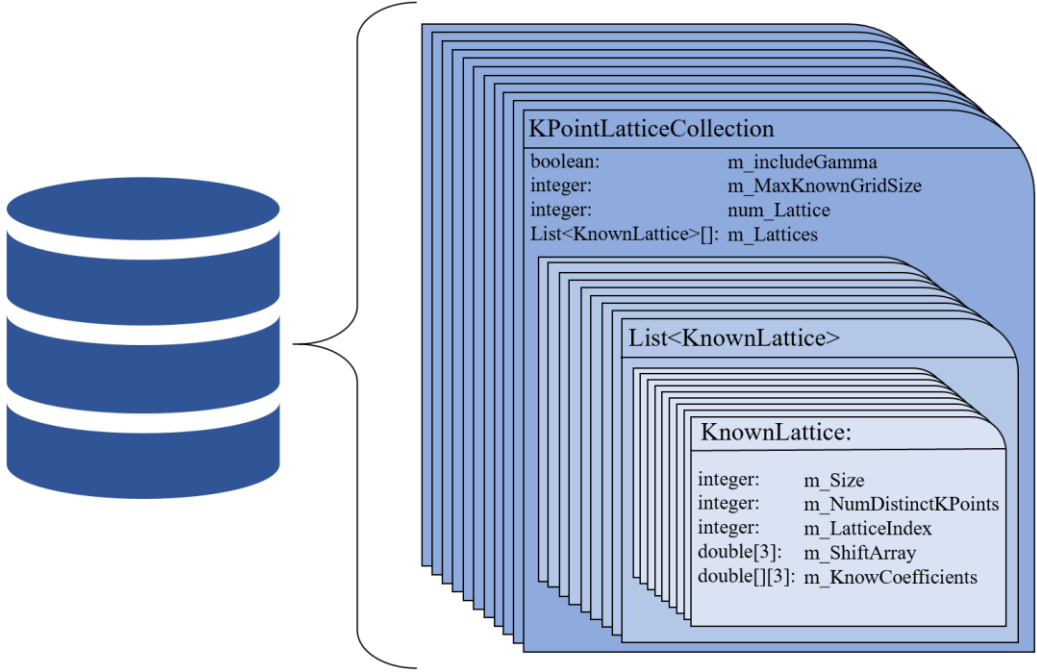


Figure 7. Schematic representation of the database organization. “m_IncludeGamma” specifies whether the grids in this file contain the Γ point. “m_MaxKnownGridSize” indicates the maximum size of the grids. “num_Lattice” is the total number of k -point grids stored in this file. “m_Lattices” is an array of lists of grids. Grids with the same N_i are stashed in the same list, and the lists are ordered by N_i . Each “KnownLattice” entry in the list represents a k -point grid. “m_Size” and “m_NumDistinctKPoints” represent the total number of k -points (N_T) and the number of symmetrically irreducible k -points (N_i). “m_LatticeIndex” is a unique index assigned to each superlattice for regenerating the transformation matrix in HNF, \mathbf{H} (described in section 2.1 of supplementary information). “m_ShiftArray” stores the shift vector for the grid in coordinates of the reciprocal lattice for the conventional primitive cell. “m_KnownCoefficients” is an array of coefficients for quickly determining an upper bound for $r_{lattice}$.

2.7 Scale Factor for Fast Generation of Large K -point Grids

For grids with a large number of total k -points, a fully dynamic search is computationally expensive, especially for the triclinic crystal system. To compromise between the speed and grid quality, we introduced scale factor in section II. D of our previous work [5]. When scale factor is used, maximum search depths will be set for each type of the seven crystal systems and they are also assigned as the initial value for N_{upper} . If the dynamic search hasn’t found the best grid before reaching the maximum search depth, the search increments the scale factor (which starts as $n=1$) and attempts to find the best “scaled” real-space superlattice for which $r_{lattice} > r_{min}/n$ and $N_T > N_{min}/n^3$. If such a scaled superlattice is found, a grid based on $n \times n \times n$ superlattice of the scaled lattice is returned. If no scaled superlattice can be found

that satisfies the constraints, n is incremented by 1 again and the process repeats. The use of the scale factor is optional for dynamic searches, but the database search method adopts the scale factor technique by default and it cannot be turned off because of the finite size of the database. Additional details on how scale factors are used are provided in section 1 of the supplementary information.

3. Implementations

Three implementations are provided to meet the diverse demands of users.

3.1 *K*-Point Grid Server: A Ready-to-use Online Application

The *K*-Point Grid Server, referred as “the server” below, is a ready-to-use internet-based application. It generates the optimal generalized Monkhorst-Pack grids by dynamic grid generation for triclinic and monoclinic systems, and by rapidly searching a pre-generated database, as discussed in section 2.6, for all other crystal systems. The database contains generalized k -point grids calculated from all symmetry-preserving superlattices of a set of 16,808 sample structures in cubic, hexagonal, trigonal, tetragonal, and orthorhombic crystal systems with different lattice parameters. The ratio of the longest conventional lattice vector to the shortest one is up to 64. Such dense sampling of the possible lattice parameters should make the database comprehensive enough to cover nearly all input structures from users. The maximum sizes of the superlattices are 46,656 ($36 \times 36 \times 36$) for cubic and 5832 ($18 \times 18 \times 18$) for triclinic, monoclinic, cubic and the other four crystal systems, the same as the search depths discussed in section 2.7. The scale factor is used when requests exceed these grid sizes. The database searching approach saves the computational cost of enumerating the superlattices and counting the symmetrically distinct k -points in corresponding grids for every user request, which gives it an advantage over dynamic grid generation. For monoclinic and triclinic systems, however, the server uses the dynamic searching scheme, since the database searching approach wouldn’t be as beneficial as it is to the other five Bravais lattices because of the huge number symmetry-preserving superlattices for these two systems. An algorithm for detecting vacuum spaces and correspondingly adjusting the k -point grid is also implemented in the server (section 3 of the supplementary information), as are other algorithms for determining symmetry that are specific to the *ab initio* software package being used.

Users can tailor their requests to the server through a set of parameters defined in a file named “PRECALC”, and the server is queried using a small script called “getKPoints”. Grid sizes are specified

through either MINDISTANCE or MINTOTALKPOINTS, which correspond to r_{min} and N_{min} respectively. An example of a PRECALC file, the getKPoints script, and a detailed description of all allowed parameters in PRECALC can be found on our website (<http://muellergroup.jhu.edu/K-Points.html>).

3.2 K-Point Grid Generator: An Open-source, Stand-alone Application

The K-Point Grid Generator is a self-contained application for users with runtime environments that might not have an internet connection. It has the exact same set of functionalities as the server and is updated accordingly every time a new version the server is released. Users still specify parameters through a PRECALC file and launch the application through a script getKPoints. But the script is different from the one used for server and is tailored for the stand-alone application. The Java programming language is used to ensure the portability and a consistent performance across operating systems. The project is open sourced through a public repository (<https://gitlab.com/muellergroup/k-pointGridGenerator>). A pre-built binary can be downloaded from our website and is packaged with the tailor calling script getKPoints and with a complete set of files for the database. The database files are stored in binary, gzipped format and take up about 7.15 MB of disk space.

3.3 KpLib: A Lightweight, Open-source C++ Library

KpLib is a lightweight library, which implements the dynamic generation approach described in sections 2.1 to 2.5 and the scale factor technique in section 2.7. The C++ programming language is chosen to make interfacing with other programming languages easier, and thus help integrate with computational materials software packages. A python module, kpGen, is also provided as a wrapper of the C++ library. The source code only contains 1122 lines, and the API uses elementary data structures as argument types, which should be available in most programming languages and easy to write wrapping functions for. We have written a demonstration application, integrated with *spglib* [31], to show how to work with the API. The library is also open sourced and a documentation of the API is provided on the homepage of its public repository (<https://gitlab.com/muellergroup/kplib>).

4. Benchmarks

Measurement of the acceleration effect of using r_{min} as a pre-screening factor is firstly presented. Then, the speed performance of the dynamic grid generation method and the database lookup method are compared. Next, the overall performance of the stand-alone application in Java and the demonstration application of kpLib in C++ are benchmarked. At last, comparisons of grid quality between our tools and GRkgridgen are given [27, 28]. All benchmarks were performed on the 102 structures randomly selected from the Inorganic Crystal Structure Database (ICSD) used in our previous work [5, 35]. Version 2019.09.17 for kpLib and version 2019.08.01 for the standalone application were used for all benchmarks.

4.1 Acceleration with r_{min} Being the Limiting Factor

The algorithms for enumerating symmetry-preserving superlattices in section 2.3 are accelerated by enforcing $r_{lattice} > r_{min}$ at each step of constructing a superlattice. This allows the algorithm to skip many superlattices at an early stage. To measure the degree of acceleration by screening based on r_{min} , we benchmarked the computation time for generating a generalized k -point grid for both Γ -centered and shifted grids, and with both the stand-alone Java application and the demonstration application in C++ using kpLib. In each case, generalized k -point grids were generated at three values of r_{min} : 25, 50, and 75 angstroms. Each calculation was repeated five times and the average response time was recorded as the calculation time for that structure. The computation time for each crystal system is taken as the average time of structures within the 102 materials that belongs to this system. The benchmark was performed on a virtual machine with Ubuntu 18.04 operation system, and on Intel Core i7-8550U processors with a clock speed of 1.80GHz. The ratios of the computation time between non-accelerated and accelerated codes are plotted in Figure 8. Results for both the Java and C++ codes demonstrate a significant acceleration, and the amount of acceleration increases as r_{min} grows. Consistent acceleration is observed for both the Γ -centered and shifted grids. The highest ratio for the Java code is 10.6 for Γ -centered grids in the hexagonal system with r_{min} equal to 75 angstroms, and that for the C++ code is 37.4 with r_{min} equal to 75 angstroms for Γ -centered grids in trigonal system.

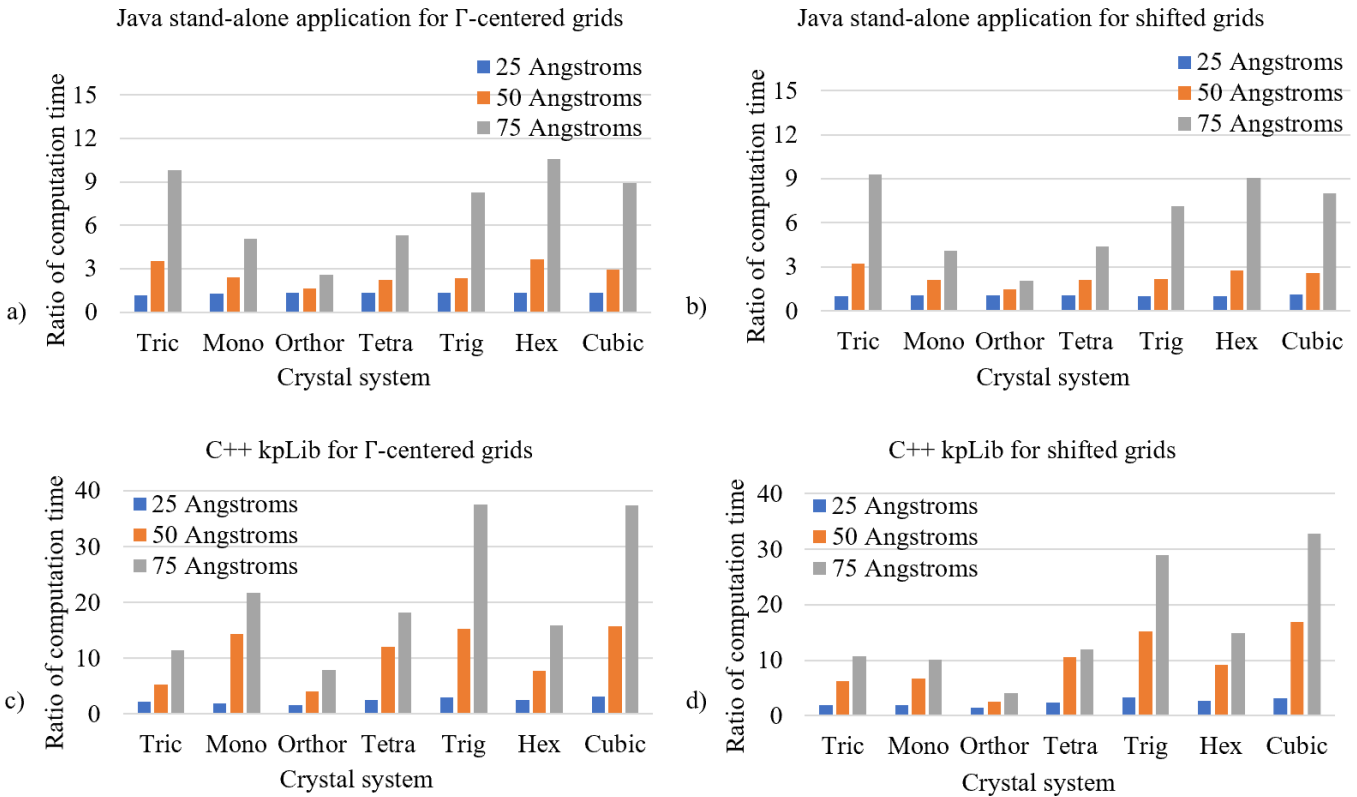


Figure 8. Ratios of computation time between the non-accelerated and accelerated algorithm for all seven crystal systems with r_{min} at 25, 50, and 75 angstroms. The top two charts illustrate results of the stand-alone application in Java, for a) Γ -centered grids and b) shifted grids. The bottom graphs demonstrate the results of the C++ application using kpLib, for c) Γ -centered grids and d) shifted grids. The x -axis lists the crystal systems. From left to right, they represent triclinic, monoclinic, orthorhombic, tetragonal, trigonal, hexagonal and cubic, respectively.

4.2 Speed Comparison between Database Lookup and Dynamic Generation

Speed benchmarks were performed on both MINDISTANCE (r_{min}) and MINTOTALPOINTS (N_{min}), representing two common ways to specify grid sizes in input files of our tools. They were also conducted for both Γ -centered grids and grids that for which the best shift vectors were automatically selected. The latter grids are referred as “auto grids” in the following. For each grid generation, three generation schemes were used: the database lookup by the stand-alone application, the dynamic search by the kpLib library and the dynamic search by kpLib library with scale factor turned on. Since the database only contains grids for the five crystal systems excluding triclinic and monoclinic ones, we performed benchmarks using the 87 out of 102 structures belonging to those five crystal systems. Each calculation was repeated three times and the average computation time was taken as the time for grid generation. The time measurement

only takes in to account the actual grid generation time and excludes the time spent for initialization and input/output operations. All benchmarks were performed on the Homewood High-Performance Cluster (HHPC) using Intel Xenon X5660 processors with a 2.80 GHz base frequency and a 48 GB RAM.

Figure 9 shows the computational time averaged over the 87 structures for both Γ -centered grids and auto grids. The range of r_{min} spans from 5 angstroms up to 100 angstroms, which is large enough for most k -point requests. We note that in our previous work [5], we found that DFT-calculated energies on all 102 materials were converged within 1 meV/atom when r_{min} reached 50 angstroms. The average times required to generate both types of grids are very close. The dynamic search by kpLib is the slowest method, taking about 2.4 seconds on average to generate both Γ -centered grids and auto grids when r_{min} is 100 angstroms. This time is significantly reduced by the use of the scale factor, which is first required (for at least one material) at 55 angstroms. The database search is the fastest for both types of grids, finishing the generation well below 1 second at all values for r_{min} . There is no significant difference in the calculation time between two types of grids for the dynamic search, while the database search for auto grids is slower than that for Γ -centered grids. This is because the dynamic search for auto grids generally has smaller N_{upper} compared with Γ -centered grids, which compensates for the time spent on iterating over multiple shift vectors. For the database lookup, there are more entries for auto grids within the database. In addition, the iteration does not have to reach N_{upper} , as the search iterates over the number of irreducible k -points rather than the number of total k -points.

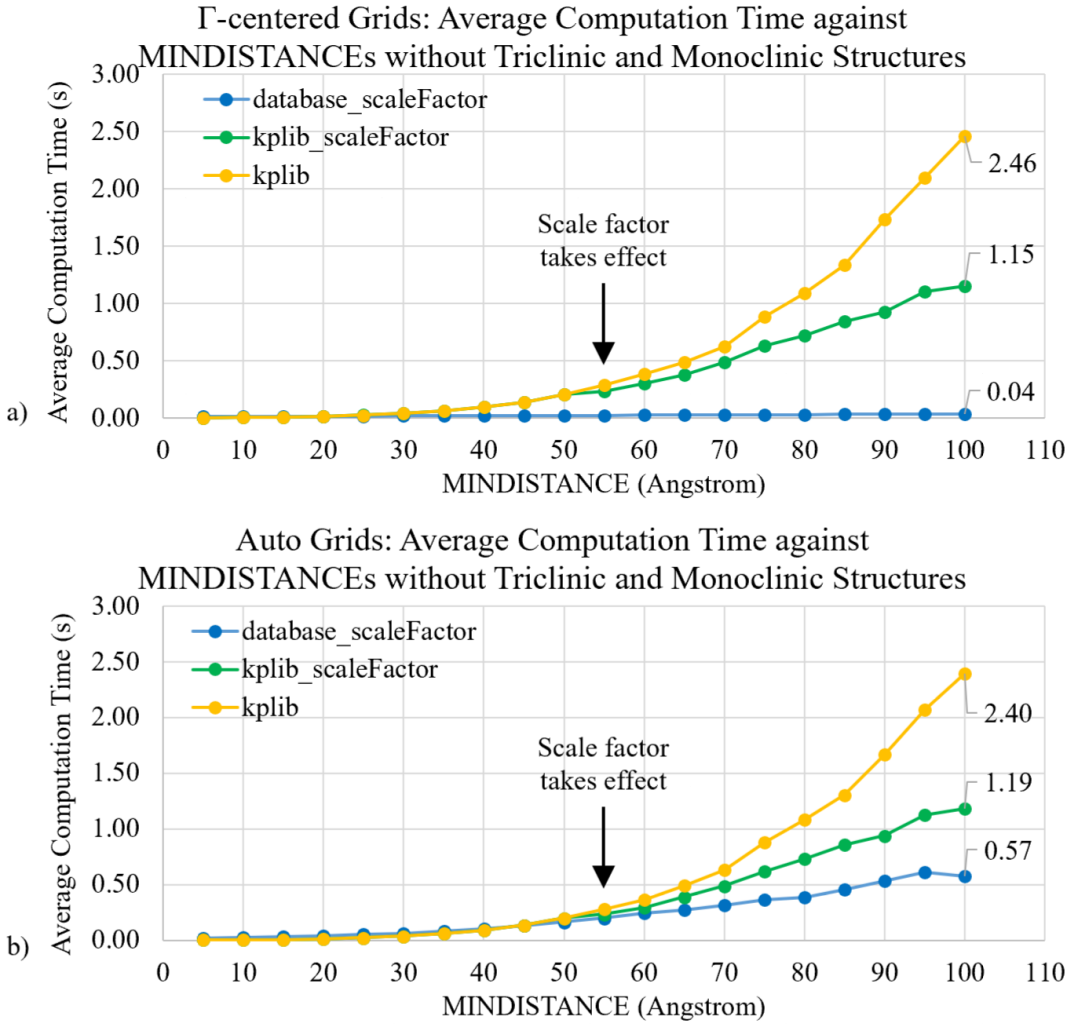


Figure 9. Average computation time of three grid generation methods over randomly selected structures without triclinic and monoclinic ones at various MINDISTANCES, for a) Γ -centered grids and b) auto grids. The largest computation time is labeled in the graphs. The smallest MINDISTANCE at which the scale factor starts to take effect is 55 angstroms. Note, not all 87 structures use scale factors at 55 angstroms, and 61 out of the 87 structures don't use scale factor even at 100 angstroms for both kinds of grids.

We have also evaluated grid-generation times based on user-specified values of N_{min} ranging from 1 to 31,622 (Figure 10). These numbers were picked randomly to give a relatively even sampling of N_{min} when plotted on a logarithmic scale. Again, the database lookup is the fastest method. The usage of the scale factor also significantly reduces the computation time for large grids. However, there are some noticeable differences with the benchmarks based on user-provided values for r_{min} . First, generating grids based on N_{min} takes more time on average than using r_{min} . In addition, the dynamic generation of Γ -centered grids,

although it has no shift vectors to iterate over, is computationally more costly. For example, the auto grids generation at $N_{min} = 7943$ complete at 6.61 seconds, while it take about 163.87 seconds for the Γ -centered case. The substantial difference in speed is because with shift vectors, the algorithm is more likely to find nearly optimal grids early in the search. Therefore, N_{upper} for dynamic generation for an auto grid is much smaller than that for Γ -centered grid generation.

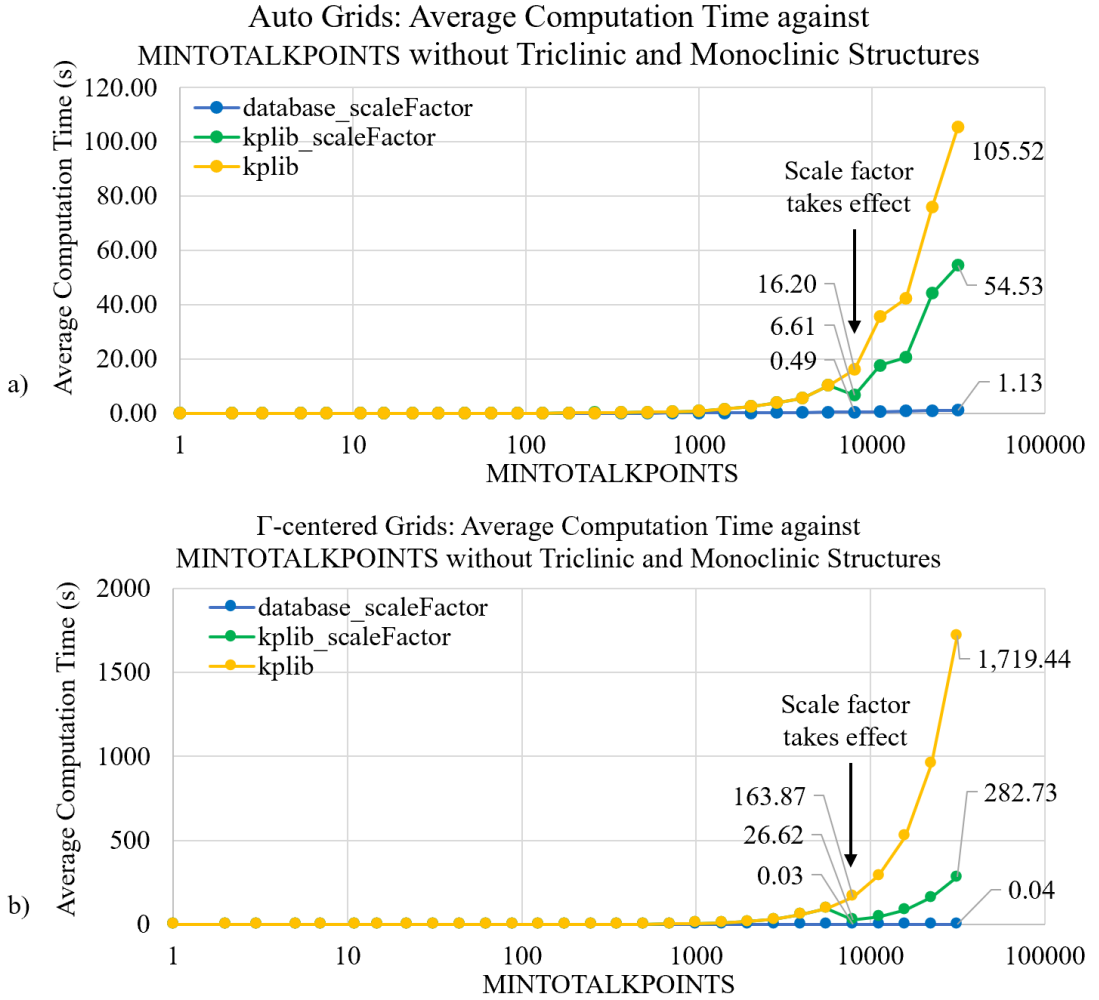


Figure 10. Average computation time of three grid generation methods over randomly selected structures without triclinic and monoclinic ones at `MINTOTALKPOINTS` ranging from 1 to 31,622 for a) Γ -centered grids, b) auto grids. The smallest `MINTOTALKPOINTS` at which the scale factor starts to take effect is 7,943. The longest computation times and the times at the value where scale factor takes effect are labeled in the graphs.

4.3 Speed Performance of Stand-alone Application and KpLib

The speed performance of the stand-alone application and kpLib with and without scale factor was benchmarked using the same procedure and hardware on the 102 randomly selected structures. This benchmark differs from the previous benchmark in that we now include the times required to dynamically generate triclinic and monoclinic grids for the standalone application. The benchmark was only performed on r_{min} , as it is faster than using N_{min} , physically more meaningful [5, 6], and thus we believe it is the most likely method to be used. All three methods have very similar performance at small r_{min} . At 50 angstroms, they can finish the generation of both types of grids in an average of less than 0.5 seconds. For large grids, the stand-alone application is the fastest because of the higher speed of the database lookup method. It takes only 0.16 second to finish the generation for Γ -centered grids at 100 angstroms and 0.73 second for auto grids. As for the dynamic search, the scale factor significantly shortens the computation time after it starts to accelerate the search beginning at 55 angstroms. At the largest r_{min} benchmarked, a full dynamic search without scale factor takes on average 4.6 seconds, while a dynamic search with the scale factor cut the time down to only about 1 second.

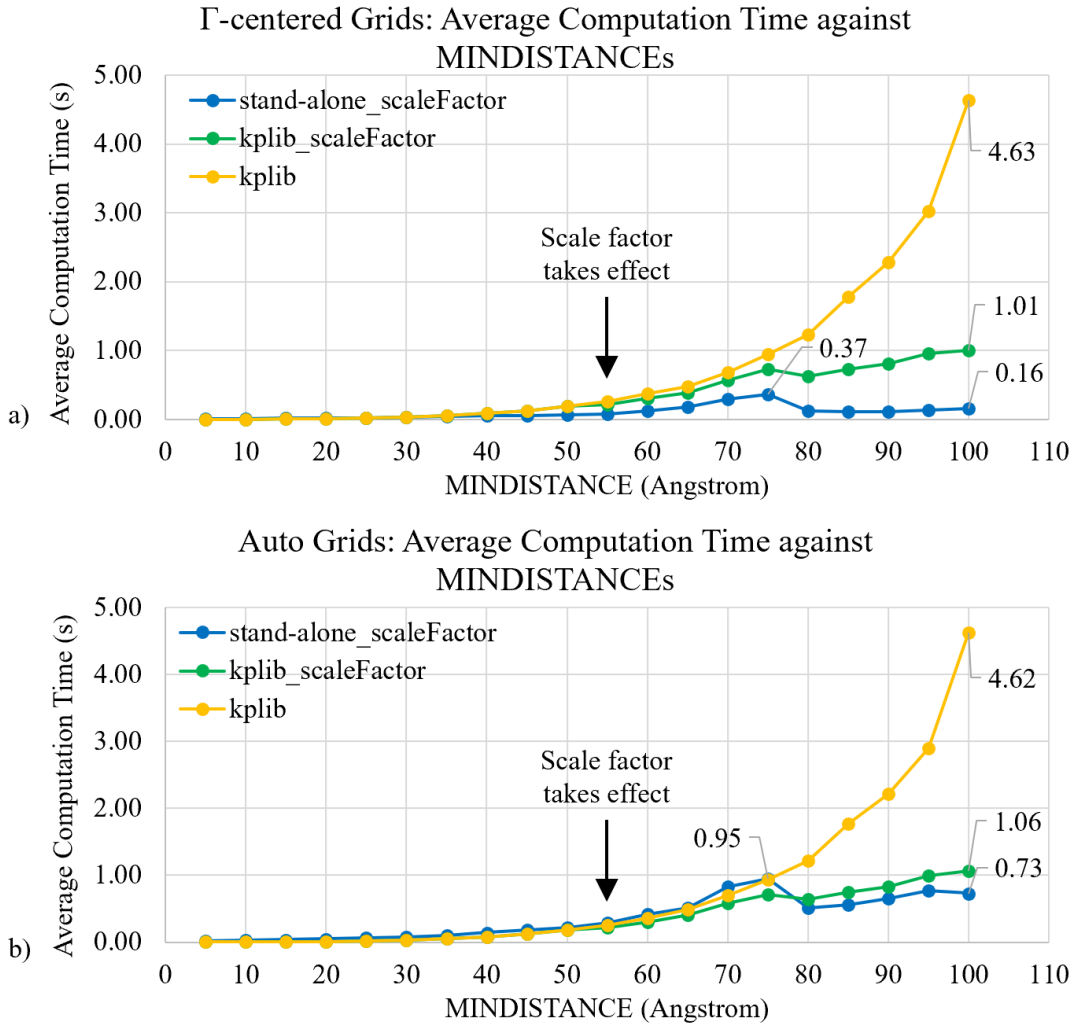


Figure 11. Average computation time of three grid generation methods at various MINDISTANCES for a) Γ -centered grids and b) auto grids. Longest computation time and the time with largest MINDISTANCE are labeled on the graphs. The smallest MINDISTANCE at which scale factor starts to have an effect is 55 angstroms. Note, not all 102 structures use scale factors at 55 angstroms and 69 out of the 102 structures don't use scale factor even at 100 angstroms.

4.4 Grid Quality Comparison between KpLib and GRkgridgen

We compared our dynamic grid generation method with GRkgridgen, another software package which can generate generalized Monkhorst Pack grids [28]. As the options for grid generation differ between the two packages, we used the following settings to make a fair comparison: both applications were instructed to select the grid with minimal N_i (a natural measure of the efficiency of a grid that meets user-provided constraints), and the required k-point density was specified by providing a value for N_{min} (defined as

MINTOTALKPOINTS in kpLib and NKPTS in GRkgridgen). In the version we tested, 0.7.5, GRkgridgen doesn't guarantee that the real-space superlattices corresponding to the returned grids satisfy $r_{lattice} \geq r_{min}$, but it does take $r_{lattice}$ into account when generating grids based on N_{min} . As kpLib only accounts for $r_{lattice}$ if r_{min} is provided by the user, to ensure a fair comparison we have constrained the grids generated by kpLib, to have $r_{lattice}$ which is at least as large as that of the grid generated by GRkgridgen at the same N_{min} and for the same structure. The same 102 structures were used for benchmarking and both Γ -centered grids and auto grids were compared. For kpLib without a scale factor, N_{min} values ranged from 1 to 5623, while for kpLib using scale factor, the range is increased to 15,848 to better demonstrate the effect of scale factor for large grids.

The scale factor makes little difference in the number of irreducible k -points for grids generated below $N_{min} = 5623$ (Figure 12). For auto grids at all values of N_{min} , including those generated using the scale factor, grids from kpLib consistently have fewer irreducible k -point than the grids from GRkgridgen on average. The same is true for Γ -centered grids generated without using the scale factor, although for very dense grids when the scale factor is used GRkgridgen may return grids that are 1-2% faster on average. The difference between kpLib and GRkgridgen is much larger for auto grids than Γ -centered grids, and it is larger for small N_T than large ones. For auto grids, which we expect to be the most commonly used mode, the expected increase in calculation speed using the grids generated by kpLib ranges from 3% to 37%.

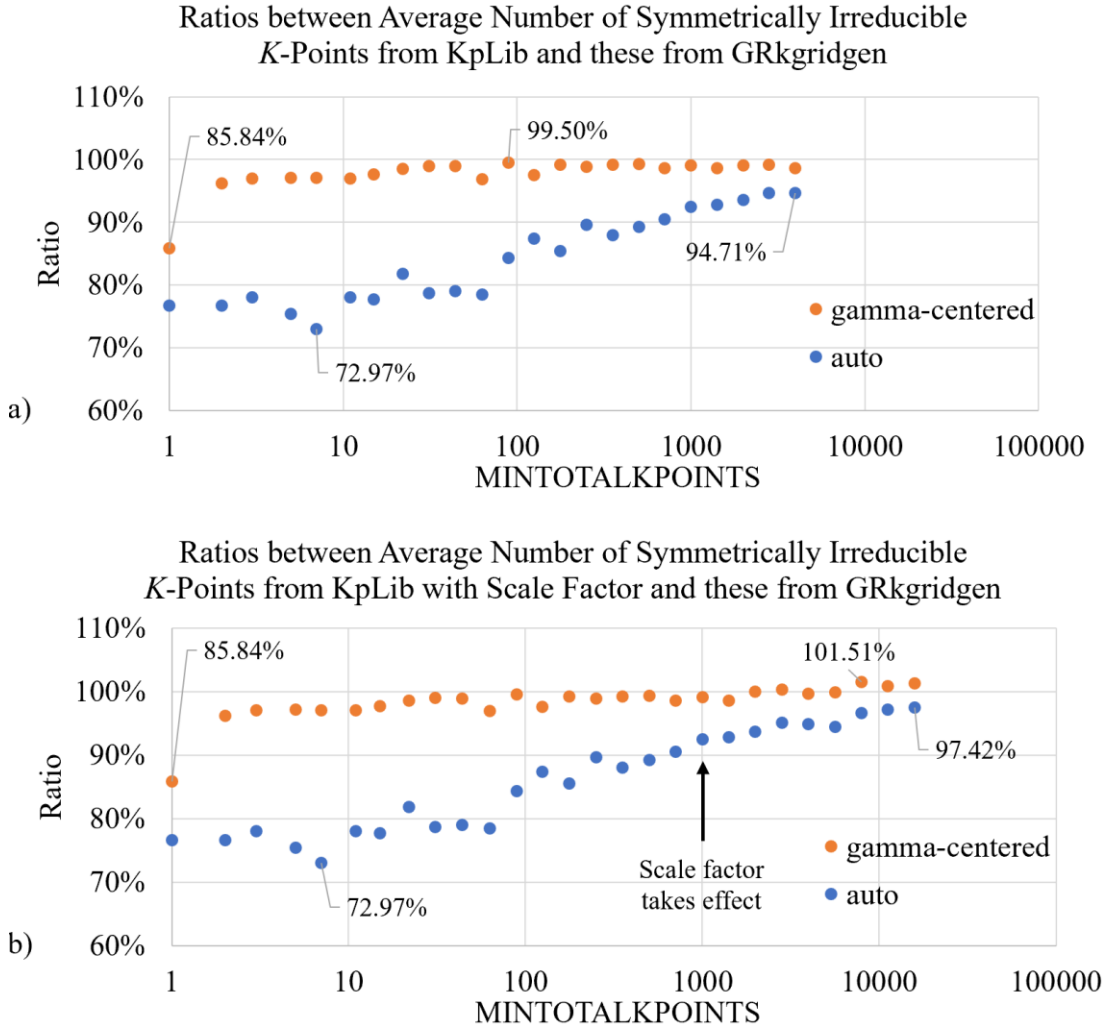


Figure 12. Ratios of average number of symmetrically irreducible k -points from the dynamic search by a) kpLib, b) kpLib with scale factor, over these from GRkgridgen, for both Γ -centered grids and auto grids. Both the maximal and minimal ratios are labeled for both types of grids. b) has a larger range of MINTOTALKPOINTS from 1 to 15848, to better demonstrate the effect of scale factor on grid qualities.

5. Conclusion

Generalized Monkhorst-Pack k -point grids have been shown to be more efficient than traditional Monkhorst-Pack grids [5, 7]. In this work, we presented core algorithms for generating optimal generalized Monkhorst-Pack grids both dynamically and through searching a pre-generated database. The rapidness of our algorithms relies on the recognition that any lattices can be decomposed into stacks of two-dimensional lattices along the primary direction of a structure, and by enforcing the constraint that $r_{lattice} \geq r_{min}$ while generating symmetry-preserving lattices. The dynamic generation scheme, which takes any combination of lower bounds for $r_{lattice}$ and N_T as inputs, can generate highly efficient k -point grids,

in the sense that it minimizes the number of symmetrically irreducible k -points within the given constraints. The algorithm we present is able to generate highly efficient generalized k -point grids for r_{min} up to 100 angstroms in less than 5 seconds on average. The dynamic generation algorithm is used to populate a database that enables even faster generation of the optimized generalized k -point grids.

Various implementations, in the forms of a web-based server (*K*-point Grid Server), a stand-alone application (the *K*-point Grid Generator), and a light-weight C++ library (kpLib), are provided to fulfil the demands of users in various computing environments. Both the *K*-Point Server and the *K*-point Grid Generator implement all the algorithms presented in this work, including the usage of dynamic grid generation for triclinic and monoclinic systems and the database-query approach for all others. KpLib implements the dynamic generation scheme and is provided for integration with *ab initio* simulation packages. The total number of lines of source code in kpLib is only 1122 so that it should be relatively easy to translate into other programming languages and implementations. The *K*-point Grid Generator and kpLib are open-sourced through online repositories.

Acknowledgements

The authors thank the National Science Foundation for the financial support under the Award No. DMR-1352373, the Homewood High-Performance Cluster (HPC) for providing computational resources, and Prof. Gus Hart for helpful discussions.

References

1. Monkhorst, H.J. and J.D. Pack, *Special Points for Brillouin-Zone Integrations*. Physical Review B, 1976. **13**(12): p. 5188-5192.
2. Ashcroft, N.W. and N.D. Mermin, *Solid State Physics*. 1976, Belmont, USA: Brooks/Cole. 132-143.
3. Tinkham, M., *Group Theory and Quantum Mechanics*. 1964, New York: McGraw-Hill Book Company. 279-281.
4. Froyen, S., *Brillouin-zone integration by Fourier quadrature: Special points for superlattice and supercell calculations*. Phys Rev B Condens Matter, 1989. **39**(5): p. 3168-3172.
5. Wisesa, P., K.A. McGill, and T. Mueller, *Efficient generation of generalized Monkhorst-Pack grids through the use of informatics*. Physical Review B, 2016. **93**(15).
6. Choudhary, K. and F. Tavazza, *Convergence and machine learning predictions of Monkhorst-Pack k-points and plane-wave cut-off in high-throughput DFT calculations*. Computational Materials Science, 2019. **161**: p. 300-308.
7. Morgan, W.S., et al., *Efficiency of Generalized Regular k-point grids*. Computational Materials Science, 2018. **153**: p. 424-430.
8. Cao, L., et al., *Mechanistic Insights for Low-Overpotential Electroreduction of CO₂ to CO on Copper Nanowires*. Acs Catalysis, 2017. **7**(12): p. 8578-8587.
9. Ding, Y. and Y. Wang, *Tunable Electronic Structures of Hydrogenated Zigzag and Armchair Dumbbell Silicene Nanosheets: A Computational Study*. The Journal of Physical Chemistry C, 2018. **122**(40): p. 23208-23216.
10. Greenman, K.P., L. Williams, and E. Kioupakis, *Lattice-Constant and Band-Gap Tuning in Wurtzite and Zincblende BInGaN Alloys*. arXiv preprint arXiv:1905.00467, 2019.
11. Hernandez, A., et al., *Fast, accurate, and transferable many-body interatomic potentials by genetic programming*. arXiv preprint arXiv:1904.01095, 2019.
12. Kratzer, P. and J. Neugebauer, *The basics of electronic structure theory for periodic systems*. Frontiers in chemistry, 2019. **7**.
13. Li, C., et al., *Improved Prediction of Nanoalloy Structures by the Explicit Inclusion of Adsorbates in Cluster Expansions*. The Journal of Physical Chemistry C, 2018. **122**(31): p. 18040-18047.
14. Liu, P., et al., *Active basal plane catalytic activity and conductivity in Zn doped MoS₂ nanosheets for efficient hydrogen evolution*. Electrochimica Acta, 2018. **260**: p. 24-30.
15. Liu, Y., et al., *Synthesis and Anisotropic Electrocatalytic Activity of Covellite Nanoplatelets with Fixed Thickness and Tunable Diameter*. ACS applied materials & interfaces, 2018. **10**(49): p. 42417-42426.
16. Lu, X., et al., *Bandgap control and optical properties of β -Si₃N₄ by single-and co-doping from a first-principles simulation*. International Journal of Modern Physics B, 2018. **32**(14): p. 1850178.
17. Nyshadham, C., et al., *Machine-learned multi-system surrogate models for materials prediction*. npj Computational Materials, 2019. **5**(1): p. 51.

18. Oses, C., et al., *AFLOW-CHULL: cloud-oriented platform for autonomous phase stability analysis*. Journal of chemical information and modeling, 2018. **58**(12): p. 2477-2490.
19. Rosenbrock, C.W., et al., *Machine-learned Interatomic Potentials for Alloys and Alloy Phase Diagrams*. arXiv preprint arXiv:1906.07816, 2019.
20. Tantardini, C. and A.A. Michalchuk, *Dess - martin periodinane: The reactivity of a λ 5 - iodane catalyst explained by topological analysis*. International Journal of Quantum Chemistry, 2019. **119**(6): p. e25838.
21. Williams, L. and E. Kioupakis, *BInGaN alloys nearly lattice-matched to GaN for high-power high-efficiency visible LEDs*. Applied Physics Letters, 2017. **111**(21): p. 211107.
22. Wolloch, M., D. Suess, and P. Mohn, *Influence of antisite defects and stacking faults on the magnetocrystalline anisotropy of FePt*. Physical Review B, 2017. **96**(10): p. 104408.
23. Wisesa, P., C. Li, and T. Mueller, *Materials with the CrVO₄ structure type as candidate superprototypic conductors*. 2019.
24. Williams, L. and E. Kioupakis, *BAIGaN alloys nearly lattice-matched to AlN for efficient UV LEDs*. arXiv preprint arXiv:1908.10814, 2019.
25. Wang, Z., et al., *Influence of Cu dopant on the electronic and optical properties of graphene-like ZnO monolayer*. Physica E: Low-dimensional Systems and Nanostructures, 2019: p. 113702.
26. Toher, C., C. Oses, and S. Curtarolo, *Automated computation of materials properties*. Materials Informatics: Methods, Tools and Applications, 2019: p. 181-222.
27. Hart, G.L.W., et al., *A robust algorithm for k-point grid generation and symmetry reduction*. Journal of Physics Communications, 2019. **3**(6): p. 065009.
28. Morgan, W.S., et al., *Generalized Regular k-point Grid Generation On The Fly*. arXiv preprint arXiv:1902.03257, 2019.
29. Mueller, T., *Computational studies of hydrogen storage materials and the development of related methods*, in *Department of Materials Science and Engineering*. 2007, Massachusetts Institute of Technology: Boston, Massachusetts. p. 127-132.
30. Hart, G.L.W. and R.W. Forcade, *Algorithm for generating derivative structures*. Physical Review B, 2008. **77**(22).
31. Togo, A. and I. Tanaka *Spglib: a software library for crystal symmetry search*. arXiv e-prints, 2018.
32. Giacovazzo, C., et al., *Fundamentals of Crystallography*. third ed. IUCr Texts on Crystallography. 2002, Oxford: Oxford University Press. 842.
33. Moreno, J. and J.M. Soler, *Optimal Meshes for Integrals in Real-Space and Reciprocal-Space Unit Cells*. Physical Review B, 1992. **45**(24): p. 13891-13898.
34. Nguyen, P.Q. and D. Stehlé. *Low-Dimensional Lattice Basis Reduction Revisited*. 2004. Berlin, Heidelberg: Springer Berlin Heidelberg.
35. *Inorganic Crystal Structure Database*. 2016, Fiz Karlsruhe. Retreived from: <http://www.fiz-karlsruhe.de/icsd.html>.

Algorithms and Code for the Generation of Generalized Monkhorst-Pack Grids

Supplementary Information

Yunzhe Wang¹, Pandu Wisesa¹, Adarsh Balasubramanian¹, Shyam Dwaraknath² and Tim Mueller^{1,*}

¹ Department of Materials Science and Engineering, Johns Hopkins University, Baltimore, Maryland 21218, USA

² Lawrence Berkeley National Laboratory, Berkeley, California, 94720, USA

E-mail: tmueller@jhu.edu

1. Using a Scale Factor for Dense Grids

We use a scale factor approach to accelerate the generation of large k -point grids (i.e. grids with a large value for N_T), which is especially beneficial for triclinic and monoclinic crystal systems.¹

The basic idea behind this approach is that rather going through the computationally expensive process of trying to find the optimal grid for some large value of N_T , we instead do a much faster

search for a grid with $\frac{N_T}{n^3}$ total k -points, where the scale factor n is a positive integer. The periodic lattice vectors for the real-space superlattice for this grid are then multiplied by n to construct a grid with N_T total k -points. This approach is necessary when generating grids using the database due to the finite size of the database, and details of how it is implemented for database-generated grids are provided in section 2.3.

¹ The symbols used in the supplementary information share the same definitions of the symbols appearing in the main text.

The scale factor is used in dynamic grid generation when the maximum search depth has been reached and no qualifying grid has been found. In this case the scale factor, which is initialized to a value of 1, is incremented and a new iteration is started with a lower bound of grid sizes calculated by

$$N_{lower} = \max \left(\frac{N_{min}}{n^3}, \left\lfloor \frac{\sqrt{2}}{2} \left(\frac{r_{min}}{n} \right)^3 / V_p \right\rfloor \right). \quad (1)$$

The upper bound is reset to the maximum search depth. When a grid satisfying all constraints is found, the upper bound is updated by:

$$N_{upper} = \frac{N_i \times N_{sym}}{n^3} \quad (2)$$

The candidate grids are all scaled by the scale factor before evaluating the values for $R_{lattice}$ and N_i used to assess grid quality.

The default maximum search depths are 729 ($9 \times 9 \times 9$), 1729 ($12 \times 12 \times 12$), 46656 ($36 \times 36 \times 36$) and 5832 ($18 \times 18 \times 18$) for triclinic, monoclinic, cubic and the other four crystal systems. Users can change these values in the code if they desire different limits. The search stops if the scale factor becomes larger than 3. Therefore, if the scale factor is used, the maximum size of a grid that can be returned is 27 times the maximum depth. If best grid is still not found, a message is displayed to remind users that the request exceeds the current maximum search capability.

Figure S1 illustrates the workflow of the dynamic search using scale factors.

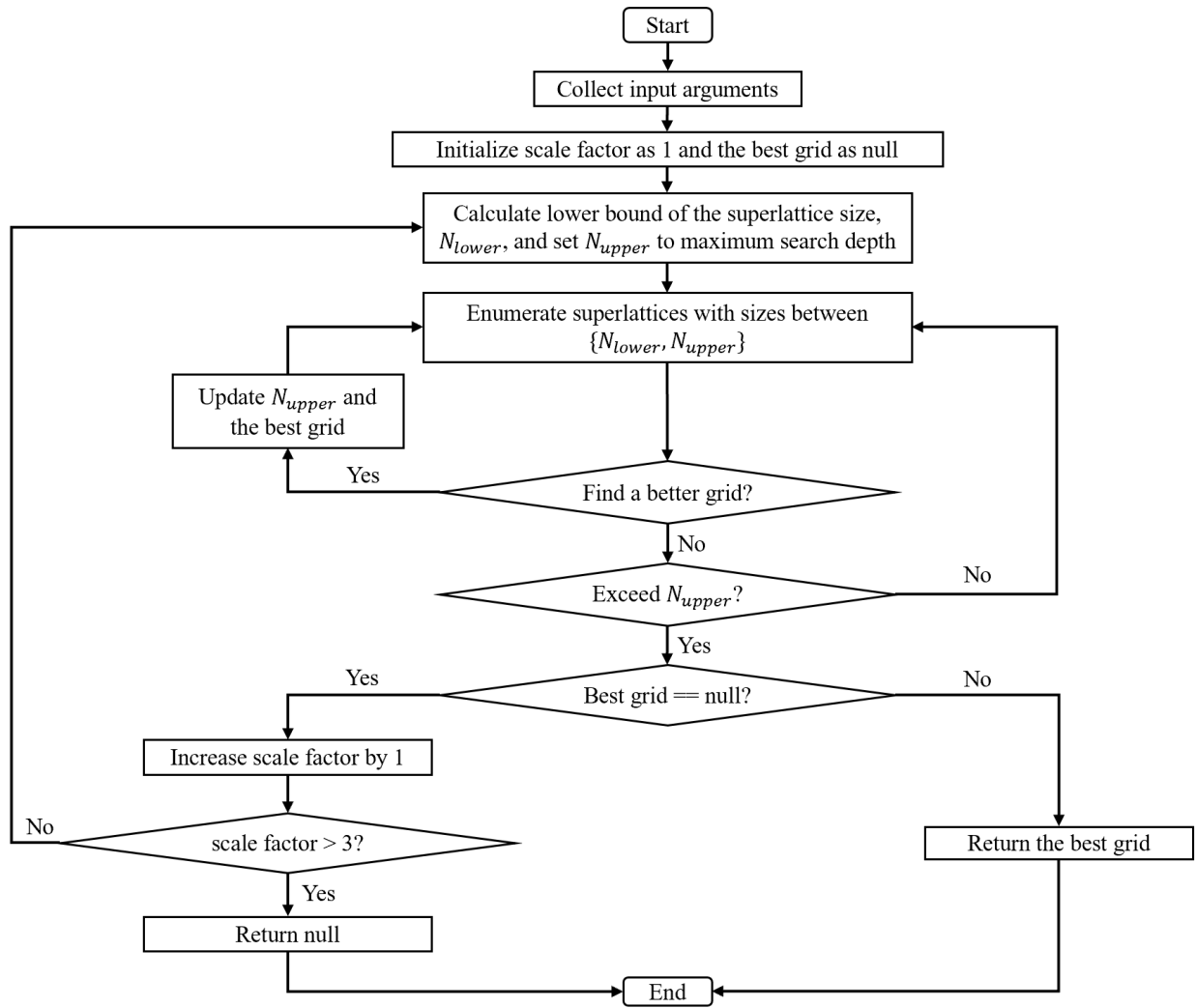


Figure S1. Workflow of the dynamic grid generation with scale factor activated.

2. Storing and Retrieving K -point Grids from the Database

In this section, we present algorithms for mapping each \mathbf{H} to a unique index and rapidly estimating $r_{lattice}$ from sets of coefficients. The workflow of the database search method is also described here in detail.

2.1 Assigning Superlattice Indices to \mathbf{H} and Regenerating \mathbf{H} from an Index

As shown by equation (2) in the main text, each k -point grid uniquely corresponds to a real-space superlattice. Section 2.3 of the main text shows that each superlattice can be uniquely represented by a transformation matrix \mathbf{H} , which is \mathbf{M} in Hermite normal form. For a given lattice size, all possible matrices in Hermite normal form can be systematically generated by enumerating all possible factor sets and, for each factor set, iterating over all possible values of the off-diagonal elements. This presents a straightforward algorithm for assigning a unique index to any matrix in Hermite normal form for which the lattice size (the determinant of the matrix) and the dimensionality (the number of rows and columns in the matrix) are known.

We first illustrate our approach via an example. Suppose we would like to generate an index for a three-dimensional superlattice of with 15 primitive cells per supercell. We start by systematically listing all the possible permutations of ways in which 15 can be factored into three integers:

$$\left\{ \begin{array}{l} \{1,1,15\}, \{1,3,5\}, \{1,5,3\} \\ \{1,15,1\}, \{3,1,5\}, \{3,5,1\} \\ \{5,1,3\}, \{5,3,1\}, \{15,1,1\} \end{array} \right\} \quad (3)$$

Each set of factors $\{f_1, f_2, f_3\}$ corresponds to the diagonal elements $\{H_{11}, H_{22}, H_{33}\}$ for the matrix in Hermite normal form. The total number of unique matrices in Hermite normal form for each set of factors is therefore given by the total number of possible combinations for the off-diagonal elements.

$$\text{number of matrices per factor set} = H_{11}^2 H_{22} = f_1^2 f_2 \quad (4)$$

For a matrix constructed from a given factor set, we can assign a unique index from 0 to $H_{11}^2 H_{22} - 1$ based on the values of the off-diagonal elements using

$$\text{index within factor set} = H_{21} + H_{31}H_{11} + H_{32}H_{11}^2. \quad (5)$$

The final index for the matrix is therefore

$$\text{index} = H_{21} + H_{31}H_{11} + H_{32}H_{11}^2 + \sum_{\substack{\text{Previous} \\ \text{factor sets}}} f_1^2 f_2. \quad (6)$$

As an example, consider the following matrix in Hermite normal form, created using the 8th factor set from those listed in equation (3).

$$\mathbf{H} = \begin{bmatrix} 5 & 0 & 0 \\ 4 & 3 & 0 \\ 0 & 2 & 1 \end{bmatrix}, \quad (7)$$

the factorizations precede the set of its diagonal elements are

$$\left\{ \begin{array}{l} \{1,1,15\}, \{1,3,5\}, \{1,5,3\}, \{1,15,1\} \\ \{3,1,5\}, \{3,5,1\}, \{5,1,3\} \end{array} \right\}. \quad (8)$$

The total number of possible HNF matrices with diagonal elements being one of these factorizations can be calculated by

$$\begin{aligned} \text{number of matrices} &= \sum_{\substack{\text{Previous} \\ \text{factor sets}}} f_1^2 f_2 \\ &= 1^2 \times 1 + 1^2 \times 3 + 1^2 \times 5 + 1^2 \times 15 + 3^2 \times 1 + 3^2 \times 5 + 5^2 \times 1 \\ &= 1 + 3 + 5 + 15 + 9 + 45 + 25 \\ &= 103 \end{aligned} \quad (9)$$

The number of matrices (inclusive) precede the given \mathbf{H} can be calculated by

$$\begin{aligned} \text{index within factor set} &= H_{21} + H_{31}H_{11} + H_{32}H_{11}^2 \\ &= 4 + 0 \times 5 + 2 \times 5^2 \\ &= 54 \end{aligned} \quad (10)$$

Therefore, the index for the given matrix is $103 + 54 = 157$.

Pseudocode for this process is provided in Figure S2. Elaboration on this pseudocode is provided as follows:

- This algorithm is applicable to any dimensions, not restricted to three.
- Line 5: each set of factors composes a possible set of diagonal elements of HNF matrices with determinant N_T . Permutations of factors are counted as different sets, since they reside on different diagonal positions of \mathbf{H} . The array of factor sets is arranged in ascending order in terms of the value of each factor. For example, for $N_T = 15$, $\{1,1,15\}$ is the first factorization. $\{1,15,1\}$ precedes $\{3,1,5\}$, since the first factor of the former factorization is smaller than that of the latter.
- Line 7 – line 10: this block counts the cumulative number of matrices that can be generated by the factor sets preceding the factor sets used to construct \mathbf{H} (equation (4)).
- Line 11: the second item of the right-hand side of the equation calculates the index of a matrix within a given factor set (equation (5)).

Algorithm 1 Assigning superlattice indices based on transformation matrices in HNF

Input:

\mathbf{H} - Transformation matrix in Hermite normal form (HNF).
 n - Dimension of the matrix.

Output:

index - Index of the superlattice.

```

1: if  $n == 1$  then
2:   return  $H_{11}$ ;
3: else
4:    $N_t = \det(\mathbf{H})$ ;
5:   factorSets[][]  $\leftarrow$  Sets of factorizations of  $N_t$  into  $n$  integral numbers;
6:   index = 0
7:   for diagonals[] in factorSets[][] do
8:     if diagonals[] ==  $\{H_{11}, H_{22}, \dots, H_{nn}\}$  then
9:       break;
10:    index = index +  $\prod_{i=1}^{n-1}$  diagonals[i] $^{n-i}$ ;
11:    index = index +  $\sum_{i=2}^n \sum_{j=1}^{i-1} [H_{ij} \cdot (\prod_{k=1}^{i-2} H_{kk}^{i-k-1}) \cdot (\prod_{k=1}^{j-1} H_{kk})]$ ;
12: return index;

```

Figure S2. Algorithm for assigning superlattice indices based on the HNF of transformation matrices. It is applicable to matrices with any dimensions.

The opposite operation, which returns a transformation matrix in HNF, can be easily derived based on the same indexing logic. The pseudocode of this opposite operation is shown in Figure S3. Take

the index calculated above as an example. The input index is 157 and determinant is 15. The index is within the index interval of the cumulative number of matrices for the factorization $\{5,3,1\}$. The rank of the matrix within this factorization is $157 - 103 = 54$. Then the off-diagonal elements can be calculated by

$$\begin{aligned} H_{32} &= 54 / (H_{11} \cdot H_{11}) = 54 / 25 = 2 \\ H_{31} &= 4 / (H_{11}) = 4 / 5 = 0 \\ H_{21} &= 4 / 1 = 4 \end{aligned} \quad (11)$$

The divisions are integer division and the remainder of each division is taken to calculate next off-diagonal element.

Algorithm 2 Regenerating the transformation matrix from an index

Input:

n - Dimension of the matrix.
 N_T - Number of total k -points.
index - Index of the superlattice.

Output:

\mathbf{H} - Transformation matrix in Hermite normal form (HNF).

Initialization:

\mathbf{H} - 3×3 zero matrix.

```

1: factorSets[][]  $\leftarrow$  Sets of factorizations of  $N_T$  into  $n$  integral numbers.
2: for diagonals[] in factorSets[] [] do
3:   count =  $\prod_{i=1}^{n-1}$  diagonals[i] $^{n-i}$ ;
4:   if index > count then
5:     index = index - count;
6:   else
7:     for i = 1 to n do
8:        $H_{ii} = \text{diagonals}[i]$ ; ▷ assign diagonal elements
9:     break;
10:   for i = n to 2 do
11:     for j = i - 1 to 1 do
12:        $c = \prod_{k=1}^{i-2} (H_{kk}^{i-k-1}) \cdot \prod_{k=1}^{j-1} (H_{kk})$ 
13:        $H_{ij} = \text{index}/c$ ; ▷ integer division
14:       index = index% $c$ ; ▷ modulo operation
15:   return  $\mathbf{H}$ ;

```

Figure S3. Algorithm for retrieving the superlattice from a given index.

2.2 Determination of Coefficients and Estimation of $r_{lattice}$

Ensuring that $r_{lattice} \geq r_{min}$ requires a calculation of $r_{lattice}$ for each candidate superlattice. Therefore, determination of $r_{lattice}$ by Minkowski reduction could become a major overhead. The database-

query approach cuts down the computational cost by remembering which linear combination of primitive lattice vectors resulted in the shortest lattice vector every time it performs a Minkowski reduction on a candidate superlattice. The next time the same generating matrix, \mathbf{H} , is encountered, the database first tries the known linear combinations of primitive vectors to see if any of them has a length less than r_{min} . If they do, the lattice can be eliminated from consideration without performing Minkowski reduction. If not, then full Minkowski reduction is performed. If a new linear combination of primitive vectors is found that has a length less than r_{min} , the coefficients of this combination are stored for future screens. In this way, the database continuously learns how to improve its performance.

The database remembers the linear combinations of primitive lattice vectors that result in a superlattice vector by projecting the superlattice vector onto a set of pre-defined mutually orthogonal vectors. For cubic, tetragonal, and orthorhombic systems, the orthogonal vectors are the conventional vectors defined in section 2.3.1 of the main text. For hexagonal and trigonal systems, the orthogonal vectors can be calculated by

$$\begin{aligned}\mathbf{v}_1 &= \mathbf{c}_1, \mathbf{v}_3 = \mathbf{c}_3 \\ \mathbf{v}_2 &= \frac{\mathbf{c}_1 \times \mathbf{c}_3}{\|\mathbf{c}_1 \times \mathbf{c}_3\|} \cdot \|\mathbf{c}_1\|\end{aligned}\tag{12}$$

where $\{\mathbf{c}_1, \mathbf{c}_2, \mathbf{c}_3\}$ are conventional lattice vectors as defined in section 2.3.1 of the main text, and $\{\mathbf{v}_1, \mathbf{v}_2, \mathbf{v}_3\}$ are the orthogonal vectors. Given a shortest lattice vector in a superlattice, \mathbf{r} , the i^{th} coefficient is calculated by

$$c_i = \frac{\mathbf{r} \cdot \mathbf{v}_i}{\mathbf{v}_i \cdot \mathbf{v}_i}\tag{13}$$

where \mathbf{v}_i is the i^{th} orthogonal vector. The opposite operation, calculating the length of a stored candidate vector in a superlattice, is accomplished by

$$\|\mathbf{r}\| = \sqrt{\sum_{i=1}^3 (c_i \cdot \|\mathbf{v}_i\|)^2}.\tag{14}$$

As the orthogonal vectors $\{\mathbf{v}_1, \mathbf{v}_2, \mathbf{v}_3\}$ need only be calculated once for any new query and the all sets of coefficients $\{c_1, c_2, c_3\}$ are stored in the database, equation (14) provides a rapid way to calculate an upper bound on $r_{lattice}$.

2.3 Grid Generation by Searching the Database

Dynamic grid generation can be slow for requests with large r_{min} and N_{min} . A pre-generated database accelerates grid generation by skipping the non-symmetry-preserving superlattices and the low quality superlattices (e.g. the ones with too many symmetrically irreducible k -points). Figure S4 provides the workflow of the database search approach for generating the optimal generalised k -point grid. It starts by estimating the lower bound of the number of symmetrically irreducible k -points:

$$N_{lower} = m_MinDistinctKPoints \left[\max \left(\frac{\sqrt{2}}{2} \cdot \left(\frac{r_{min}}{n} \right)^3 / V_p, \frac{N_{min}}{n^3} \right) \right]. \quad (15)$$

where n is the scale factor and $m_MinDistinctKPoints[]$ is an integral array created when loading a file from the database. The N -th element represents the minimum value of N_i of all the grids stored in this file that have a size of N . The minimum N that satisfies $r_{lattice} \geq r_{min}$ and $N \geq N_{min}$ is calculated by the `max()` function. The first argument is the minimum size of a superlattice that could satisfy $r_{lattice} \geq r_{min}$, and the justification of the prefactor is similar to that of equation (8) of the main text. For Γ -centered grids of all lattices and shifted grids of non-cubic lattices, the minimum volume is that of a fcc unit cell with a distance of no more than r_{min} between lattice points. For cubic systems, a fcc superlattice results in a bcc reciprocal lattice, and the only symmetry-preserving shift of the Γ point in a bcc lattices is $[0.5, 0.5, 0.5]$, which results in a Γ -centered grid. Therefore, the minimum volume of supercell for a shifted grid in a cubic system is that of the second closest-packed lattice, a body-centered-cubic (bcc) lattice [1]. N_{lower} in this case is calculated by

$$N_{lower} = m_MinDistinctKPoints \left[\max \left(\frac{4}{3\sqrt{3}} \cdot \left(\frac{r_{min}}{n} \right)^3 / V_p, \frac{N_{min}}{n^3} \right) \right]. \quad (16)$$

N_{upper} is the maximum number of N_i of grids in the database, which have the same symmorphic space group as the input structure. Grids are searched by starting with the list for which $N_i = N_{lower}$ and incrementally increasing the size of N_i until $N_i = N_{upper}$. Once an optimal lattice for a given value of N_i is found, there is no need to search for larger values of N_i . If the search cannot find a fulfilling grid before N exceeds N_{upper} , the scale factor is increased by 1, the lower bound of the search is updated, and the search restarts from the new N_{lower} . If a grid satisfying all constraints is still not found when the scale factor exceeds 3, the search stops and a message is displayed to notify the user that the request exceeds the current maximum search capability. Since the database is generated by iterating grids up to at least the search depths mentioned in section 2.6 of the main text (which are the same as the depths in section 1 of the supplementary information), the maximum search capabilities are at least 27 times 46,656 ($36 \times 36 \times 36$) for cubic systems and 27 times 5,832 ($18 \times 18 \times 18$) for the other four crystal systems in the database. The alignment of search depths between database and the dynamic search with the scale factor ensures consistent results from both types of generation approaches.

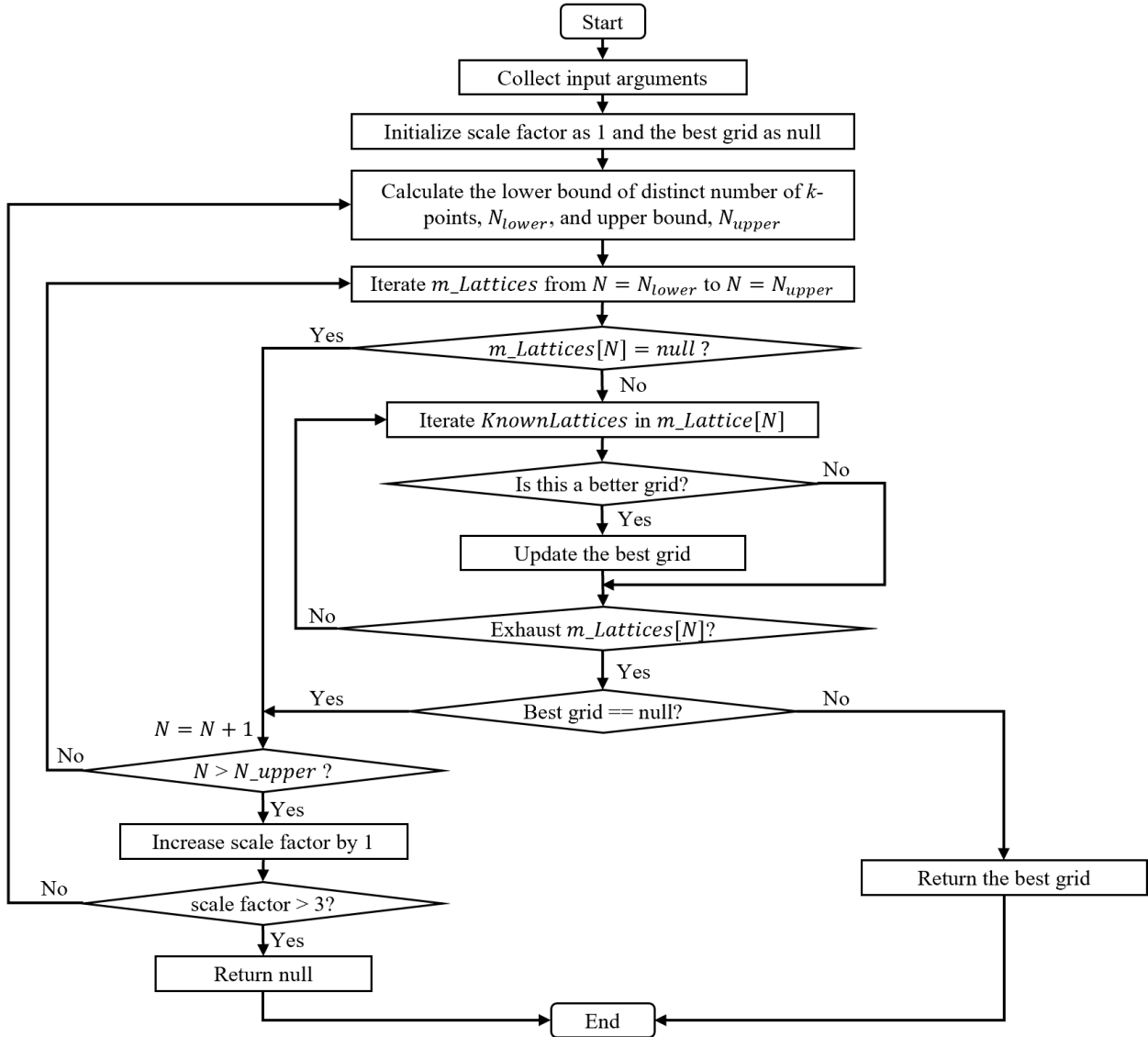


Figure S4. A diagram summarizes the grid generation workflow by the database-searching approach.

There are two situations in which the database may return slightly different grids than dynamic grid generation. The first is due to a difference in the way the scale factor is used for the database search and how it is used for dynamic grid generation. In dynamic grid generation, the optimized grid is chosen based on the value of N_i for the final returned grid. For the database search, the value of N_i for the scaled (smaller) grid is used, as the database is indexed by this value. In some cases this can result in the database returning a final grid that has a larger N_i than the grid

generated dynamically when the scale factor is used. The database may also return different results from dynamic grid generation when N_{\min} is the limiting factor in grid generation, as the database was generated using Pareto frontiers based on r_{\min} , which we expect to be the more commonly-used constraint. In both situations any difference in efficiency between the grid returned by the database and the dynamically generated grid is typically small.

3. Algorithm for Detection of Structures without 3-dimensional Periodicity

In software packages that assume three-dimensional periodicity for all calculations, low-dimensional structures such as surfaces and nanoparticles are modelled by adding vacuum to the normal directions of the periodic low-dimensional lattice. We will refer to such normal directions as the “vacuum directions”. As there is little interaction between materials separated by vacuum, it is not necessary to sample more than one k -point in reciprocal lattice directions that are normal to the real-space periodic lattice. To ensure efficient k -point grids are generated in such cases, we have developed an algorithm to determine when structures are suitably separated by vacuum, and we adjust the generated k -point grid accordingly. For example, when simulating a slab, the density of the grid will be minimized along the direction parallel to the vacuum direction. For nanoparticles, only a single k -point will be returned.

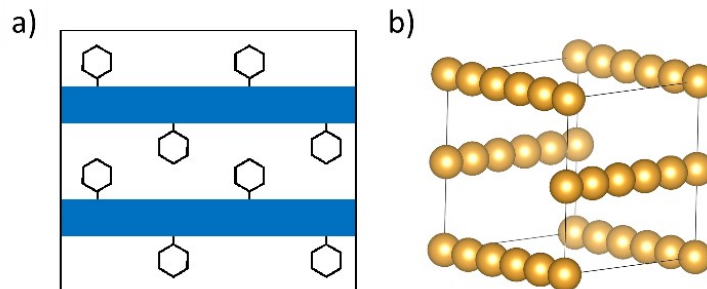


Figure S5. Two examples of low-dimensional systems recognized by our algorithm. A) A slab with adsorbed molecules. As long as the distances between all atoms in one slab (including adsorbates) and the nearest atoms in a neighboring slab (including adsorbates) is at least r_{gap} , this will be treated as a low-dimensional system. B) An example with one-dimensional chains oriented in different directions. As long as the distances between chains are at least r_{gap} , the algorithm will recognize this system as being periodic in two dimensions.

The user-provided input to our algorithm is a minimum distance by which slabs, nanowires, or surfaces must be separated to trigger a change in the k -point grid. We call this quantity r_{gap} . Given a value for r_{gap} , our algorithm identifies gaps between slabs, nanowires, or nanoparticles regardless of the topology of the system (Figure S5). We accomplish this by starting at a single atom and recursively visiting all neighbouring atoms within a distance of r_{gap} . When we encounter an atom that is translationally equivalent to an atom we have already visited, we record the vector between those atoms. We refer to such vectors, which are normal to the vacuum directions, as “contiguous vectors”. For a slab structure, the contiguous vectors will be parallel to the slab surface. In a nanowire, the contiguous vector is the lattice vector parallel with the nanowire. The contiguous vectors are not necessarily the input primitive lattice vectors but must be linear combinations of them. In some cases, (e.g a molecule between two slabs, or something like Figure S5b), there may be more than one set of contiguous atoms that are separated by at least r_{gap} . We identify such cases by ensuring that we have visited each set of translationally equivalent atoms at least once.

Algorithm 3 Detection of periodic sublattice in structures

Input:

$\mathbf{x}[], \{\mathbf{v}_i\}$ - As defined above.
 $\text{seen}[]$ - Array of boolean type. $\text{seen}[i]$ indicates whether the atom $\mathbf{x}[i]$ has been passed to the function `FINDCONTIGUOUSVECTORS()`.
 siteIndex - The index of atom for which neighbouring atoms are searched.
 precision - This value is used to address numerical error. Distance with an absolute value below precision are treated as if they are zero.

Output:

$\{\mathbf{v}_i\}$ - Contiguous vectors.

```
1: function GETCONTIGUOUSVECTORS( $\mathbf{x}[], \text{seen}[], \{\mathbf{v}_i\}$ )  
2:   for  $i = 1$  to  $\mathbf{x}.\text{length}$  do  
3:     if  $\text{seen}[i]$  then  
4:       continue;  
5:     else  
6:        $\text{seen}[i] = \text{true}$ ;  
7:        $\{\mathbf{v}_i\} = \text{FINDCONTIGUOUSVECTORS}(\mathbf{x}[], \text{seen}[], i, \{\mathbf{v}_i\})$ ;  
8:   return  $\{\mathbf{v}_i\}$ ;  
  
9: function FINDCONTIGUOUSVECTORS( $\mathbf{x}[], \text{seen}[], \text{siteIndex}, \{\mathbf{v}_i\}$ )  
10:    $\mathbf{y}[] \leftarrow$  array of neighbouring atoms of  $\mathbf{x}[\text{siteIndex}]$ , within a radius of  $r_{\text{gap}}$ ;  
11:   for  $j = 1$  to  $\mathbf{y}.\text{length}$  do  
12:      $k \leftarrow$  index in  $\mathbf{x}[]$  of the translationally equivalent atom of  $\mathbf{y}[j]$ ;  
13:     if not  $\text{seen}[k]$  then  
14:        $\text{seen}[k] = \text{true}$ ;  
15:        $\{\mathbf{v}_i\} = \text{FINDCONTIGUOUSVECTORS}(\mathbf{x}[], \text{seen}[], k, \{\mathbf{v}_i\})$ ;  
16:     else  
17:        $\mathbf{u} = \mathbf{y}[j] - \mathbf{x}[k]$ ;  
18:       if  $\|\mathbf{u}\| < \text{precision}$  then  
19:         continue;  
20:       else if not parallelToLatticePlane( $\mathbf{u}, \{\mathbf{v}_i\}$ ) then  
21:         add  $\mathbf{u}$  to  $\{\mathbf{v}_i\}$ ;  
22:       if  $\mathbf{v}.\text{length} == 3$  then  
23:         return  $\{\mathbf{v}_i\}$ ;  
24:   return  $\{\mathbf{v}_i\}$ ;
```

Figure S6. Algorithm for detection of the periodic sublattice in structures without periodicity in three dimensions.

This algorithm is shown by the pseudocode in Figure S6. Elaboration on some lines are provided as follows:

- Function `FINDCONTIGUOUSVECTORS()`: constructs the contiguous vectors recursively by crawling over all atoms that are separated from at least one other atom in the set by a distance no more than r_{gap} . When an atom that is translationally equivalent to one that has previously been visited is found, then the vector between these atoms is a candidate vector.

It is added to the set of contiguous vectors if it is not spanned by the ones already in the set.

- GETCONTIGUOUSVECTORS() ensures that all atoms in the unit cell are visited by FINDCONTIGUOUSVECTORS(). This is important for situations in which there are multiple sets of contiguous atoms separated by at least r_{gap} (e.g. a molecule above a slab, or something like Figure S5b).

Once we have identified the contiguous vectors, the vacuum direction(s) are calculated as the directions that are normal to all contiguous vectors. The algorithm then distorts the input structure by stretching the primitive lattice vectors along the vacuum directions so that their projections along the vacuum directions have sizes at least r_{min} ($2r_{min}$ for nanowires and slabs). The components of the lattice vectors parallel to the contiguous vectors are not changed. This effectively tells the lattice-generation algorithm that spacing between translationally equivalent atoms is already sufficiently large in the vacuum directions, and supercells only need to be created in the directions parallel to the contiguous vectors. The grid-generation algorithm is used on the distorted structure. The coordinates of the generated k -points, in the basis of reciprocal lattice vectors, are the same for both the original and distorted structure. Through this approach we are able to generate low-dimensional grids that respect the symmetry of the three-dimensional calculation. The complete algorithm is summarized as pseudocode in Figure S7. Explanations for some lines are presented as follows:

- Line 3: V_{min} represents the minimum supercell volume. It's equal to the volume of a primitive unit cell, V_p , times the minimum number of total k -points, N_{min} , that users specify.
- Line 4 – line 11: $r_{stretch}$ is the target distance by which the projections of primitive lattice vectors along the vacuum directions should be stretched to. This block demonstrates how to calculate this value for various periodicities. For $n = 0$, $r_{stretch}$ is equal to the larger value between r_{min} and the maximum possible value of $r_{lattice}$ for a unit cell volume of V_{min} . The latter is achieved when the lattice is close-packed with a fcc structure. For $n = 1$, line 7 gives the minimum length of the real-space superlattice vectors parallel to the one-dimensional structure. Line 13 then calculates $r_{stretch}$ by finding the larger value between

r_{min} and the maximum possible value of $r_{lattice}$ for a two-dimensional lattice with primitive cell area of $V_{min} / r_{periodic}$. The latter is achieved for a hexagonal lattice. For $n = 2$, line 10 calculates the maximum of 1) the minimum cell area for a planar lattice for which $r_{lattice}$ is at least r_{min} and 2) the cell area for the lattice formed by the found contiguous vectors. The area given by 1) can be calculated by assuming the 2-dimensional lattice is hexagonal.

- Line 13 – line 15: this code block calculates a uniform scaling ratio for all lattice vectors. The maximum ratio is selected to ensure the projections of all lattice vectors along vacuum directions have a length at least $r_{stretch}$.

Algorithm 4 Adjusting structures without three-dimensional periodicity

Input:

$\mathbf{x}[]$ - Array of atomic coordinates in the basis of $\{\mathbf{a}'_1, \mathbf{a}'_2, \mathbf{a}'_3\}$.
 r_{gap} - Minimum gap size between atoms, larger than which a gap is considered as a vacuum.
 N_{min} - The minimum number of total k -points specified by users.
 $\{\mathbf{a}_1, \mathbf{a}_2, \mathbf{a}_3\}$ - Primitive lattice vectors.
 V_p - Volume of the primitive unit cell.

Output:

$\{\mathbf{a}'_1, \mathbf{a}'_2, \mathbf{a}'_3\}$ - Stretched lattice vectors whose projections along the vacuum directions having sizes at least the $2 \times r_{min}$.

Initialization:

$\{\mathbf{v}_i\}$ - An empty array of contiguous vectors.
 $\text{seen}[]$ - An array of boolean type with $\mathbf{x}.\text{length}$ elements initialized as *false*.

```

1:  $\{\mathbf{v}_i\} = \text{GETCONTIGUOUSVECTORS}(\mathbf{x}[], \text{seen}[], \{\mathbf{v}_i\});$ 
2:  $n \leftarrow \text{dimensions of } \{\mathbf{v}_i\};$ 
3:  $V_{min} = V_p \times N_{min};$ 
4: if  $n == 0$  then
5:    $r_{stretch} = \max(r_{min}, \sqrt[3]{V_{min}/\sqrt{2}});$ 
6: else if  $n == 1$  then
7:    $r_{periodic} = \max(r_{min}, \|\mathbf{v}\|);$ 
8:    $r_{stretch} = 2 \times \max(r_{min}, \sqrt{(2\sqrt{3})/3 \cdot V_{min}/r_{periodic}});$ 
9: else if  $n == 2$  then
10:    $S_{periodic} = \max(\sqrt{3}/2 \cdot r_{min}^2, \|\mathbf{v}_1 \times \mathbf{v}_2\|);$ 
11:    $r_{stretch} = 2 \times \max(r_{min}, V_{min}/S_{periodic});$ 
12:  $\text{scalingRatio} = 0;$ 
13: for  $\mathbf{a}_i$  in  $\{\mathbf{a}_1, \mathbf{a}_2, \mathbf{a}_3\}$  do
14:    $\mathbf{n}_i \leftarrow \text{projection of } \mathbf{a}_i \text{ to the normal directions of lattice } \{\mathbf{v}_i\};$ 
15:    $\text{scalingRatio} = \max(\text{scalingRatio}, r_{stretch}/\|\mathbf{n}_i\|);$ 
16:    $\{\mathbf{e}_i\} \leftarrow \text{unit vectors normal to } \{\mathbf{v}_i\};$ 
17:   for  $\mathbf{a}_i$  in  $\{\mathbf{a}_i\}$  do
18:     for  $\mathbf{e}_j$  in  $\{\mathbf{e}_i\}$  do
19:        $\mathbf{a}'_i = \mathbf{a}_i + [(\text{scalingRatio} - 1) \cdot (\mathbf{a}_i \cdot \mathbf{e}_j)] \cdot \mathbf{e}_j;$ 
20: return  $\{\mathbf{a}'_1, \mathbf{a}'_2, \mathbf{a}'_3\};$ 

```

Figure S7. Algorithm for stretching lattice vectors to reduce k -point density along the vacuum directions accordingly.

References

1. Giacovazzo, C., et al., *Fundamentals of Crystallography*. third ed. IUCr Texts on Crystallography. 2002, Oxford: Oxford University Press. 842.